NATIONAL ADVISORY COMMITTEE FOR AERONAUTICS

TECHNICAL MEMORANDUM 1299

ADDITIONAL MEASUREMENTS OF THE DRAG OF SURFACE

IRREGULARITIES IN TURBULENT

BOUNDARY LAYERS

By W. Tillmann

Translation of ZWB Untersuchungen und Mitteilungen Nr. 6619,
December 27, 1944

NACA

Washington
January 1951

NATIONAL ADVISORY COMMITTEE FOR AERONAUTICS

TECHNICAL MEMORANDUM 1299

ADDITIONAL MEASUREMENTS OF THE DRAG OF SURFACE

IRREGULARITIES IN TURBULENT

BOUNDARY LAYERS[*]

By W. Tillmann

ABSTRACT

In connection with earlier measurements by K. Wieghardt the increase of the turbulent friction drag was determined for some additional types of common surface irregularities.

1. SYMBOLS

X   distance downstream from the leading edge of the plate

y   perpendicular distance from the plate

z   coordinate of the plate span

u   velocity in the boundary layer

U   free-stream velocity

ρ density

$q = \frac{1}{2}\rho u^2$ dynamic pressure in the boundary layer

$Q = \frac{1}{2}\rho U^2$ free stream dynamic pressure

δ boundary-layer thickness

h   height of irregularity

t   depth of cavity

L   width of irregularity

f   frontal area of the irregularity (projection on a plane
              normal to the direction of flow)

F   plane area of irregularity

$$\bar{u} = \frac{1}{h} \int_0^h u(y) \, dy \quad \text{mean velocity in the boundary layer between } y = 0 \\ \text{and } y = h$$

$$\bar{q} = \frac{1}{h} \int_0^h q(y) \, dy \quad \text{mean dynamic pressure in the boundary layer} \\ \text{between } y = 0 \text{ and } y = h$$

Δw difference between plate drags with and without irregularity

$$\left.\begin{array}{l} C_w = \dfrac{\Delta w}{\bar{q}f} \\[2mm] c_w = \dfrac{\Delta w}{Qf} \\[2mm] \Delta c_w = \dfrac{\Delta w}{QF} \end{array}\right\} \text{drag coefficients}$$

ν kinematic viscosity

$$\left.\begin{array}{l} Re(X) = \dfrac{UX}{\nu} \\[2mm] Re(h) = \dfrac{\bar{u}h}{\nu} \end{array}\right\} \text{Reynolds numbers}$$

2. INTRODUCTION

The calculation of the turbulent skin friction of smooth surfaces is a task which can usually be solved with sufficient accuracy and offers special difficulties only when strong positive pressure gradients exist. The additional resistance which single roughness elements (for instance, projections and indentations) produce has been systematically investigated by K. Wieghardt (reference 1). Further measurements became necessary since, for certain common surface irregularities, reference 1 provides only inadequate data or no data at all.

The present investigation is concerned, among other things, with continuously rounded projections, the resistance of which depends mainly on the Reynolds number, with the influence of irregularities lying behind one another, and with indentations of various forms.

3. EXPERIMENTAL ARRANGEMENT

The apparatus and methods were as described in reference 1. The upper wall of the roughness channel was again so adjusted that, along the whole experimental surface (lower wall), conditions of a flat plate in a free stream were produced. The difference between the drags of a rectangular measuring plate (500 × 300 mm^2) which was in a section of the bottom plate (1.4 × 6 m^2) but which was separately supported on a drag balance, with and without irregularities attached, was the desired drag increment.

With this arrangement not only the pressure drag of the roughness elements but also any associated change in the surface friction was determined. Larger roughness elements, which produced a persistent wake, had to be moved forward about the length of the measuring plate in order to ascertain the total drag to be assigned to the element.

For practical reasons, a similar forward displacement of the indentation elements (where, however, the wake was much less pronounced) was not tried.

The balance measurements were made at a stream velocity U ≈ 17.8 meters per second for two different locations of the roughness element behind the plate leading edge, X ≈ 0.4 meter and 4.4 meters. At these test positions the boundary layer thickness δ amounted to 14 millimeters and 78 millimeters, respectively, and the Reynolds number Re(X) = UX/ν to 4.6 × 10^5 and 5.2 × 10^6, respectively. The undisturbed velocity profile could be approximated quite well by the 1/7-power law.

4. RESULTS

The surface irregularities investigated are presented on pages 12 and 13. The resulting measurements, together with the most important experimental data, are given in figures 1 to 26.

In order to eliminate the dependence of the measurements on the velocity distribution of the experimental stream, K. Wieghardt (reference 1) generalized the definition of the drag coefficient and the Reynolds

number of the disturbing element by introducing a mean dynamic pressure
and a mean velocity. These definitions are contained in the list of
symbols, but values can be obtained easily, if necessary, with the aid
of figure 27 from the corresponding undisturbed dynamic pressure. An
explanation of the individual figures, in which the results are
collected and compared with other measurements, will be given in what
follows.

Figures 1 and 2: The suitability of the generalized drag coef-
ficient is confirmed for square plates arranged perpendicular to the
stream along a flat plate.

If $h/\delta > 1$ the change in plate surface friction drag is small
relative to the pressure drag, and one may expect the same value for
C_W as with uniform flow. Flachsbart (reference 2), on the basis of
extensive recent data, has obtained $c_W = 1.16$ for square plates in
a free stream; in satisfactory agreement with this value, there results
from measurements in the boundary layer at the forward position
$C_W = 1.14$, and similar experiments by Engelhardt (reference 3) likewise
give $C_W = 1.14$.

If, however, the plate is submerged in the boundary layer, then,
on the one hand the change in the surface drag, which is a function
of the position $Re(X)$, becomes more important and, on the other hand,
the boundary layer next to the wall influences the whole flow around
the disturbing body, whence C_W becomes a function of $Re(h)$.

Figures 3 and 4: As soon as the flow leaves the rear end of the
bar without too much eddy formation, the negative pressure behind the
bar decreases. Therewith a drag decrease occurs which depends only
slightly on the Reynolds number.

Similar studies of the drag coefficients of similar disturbances
allow us to see the influence of varying geometric forms and make
possible estimations of the drag coefficients of still other designs.

Figures 5, 6, and 7: On rounded disturbances, for which the point
of separation is not fixed by sharp corners, Wieghardt found, for the
turbulent boundary layer in flow along a flat wall, sharp decreases in
drag coefficients similar to those observed in the free stream. The
flatter the roughness element, the smaller the critical Reynolds number.
Therefore the measurements on hoods, half bodies of revolution, tear-
drop shapes, etc., give very different drag coefficients. In comparison
with spherical segments (reference 1, fig. 45) one can conclude from
the small C_W values for the hoods investigated in the present
experiment that these were measured for the most part at supercritical
stream conditions.

In figure 5, for comparison, corresponding measurements on half bodies of revolution by Engelhardt (reference 3) are included. For these, C_w increases strongly in an unexpected manner at large t/h values. In these cases, where the affixed roughness elements extend over almost the whole length of the measuring plate, which was suspended in the free stream of a wind tunnel, probably the stagnation point flows and the wake changed so greatly that a wholly different flow resulted.

The curvature of the forward part of the roughness element seems to exert a strong influence on the location of the separation point. The drag coefficients of the tear-drop shapes are not to be compared directly since these were obtained from experiments on a fuselage surface. If one broadens the after part of the hoods a flat minimum for the drag coefficient is found in good agreement with reference 3.

Figures 8 and 8a: The drag of a faired flat ridge shows the behavior expected from the preceding remarks.

If two of these ridges with one behind the other are investigated at below critical $Re(h)$, the downstream ridge produces only a part of the drag of the same ridge in the undisturbed stream as long as it lies in that part of the boundary layer disturbed by the forward ridge. At the slightly above-critical $Re(h)$ number 7.1×10^3 the drag of the forward ridge decreases, to be sure; however, the downstream ridge in the wake region becomes, as a consequence of the decreased velocity, subject to a subcritical stream and has, at a certain distance from the forward ridge, a considerably larger resistance than the forward ridge. At $Re(h)$ considerably in excess of the critical this effect is naturally no longer to be expected. The downstream ridge first reaches the above-critical C_w values at the end of the mutual influence zone (see example).

One can apply these results generally to rounded single roughness elements lying one behind another (for example: rows of brazier-head rivets).

Figures 9 and 10: Since three-dimensional roughness elements, because of the lateral flow around them, produce only a very limited dead-water region, countersunk rivets lying in rows one behind the other influence each other only when they are grouped very closely. In addition to the two transverse rows arranged at varying distances from one another, six rows, one behind the other, with $A/D = 2.5$ and $B/D = 2.0$ were investigated. Then the drag coefficient differed from that of the rivet head measured alone only within admissible scatter, even independent of whether any following rivet was directly behind or halfway between the preceding rivets.

One may expect these results from the Schlichting investigations (reference 4). The chosen pattern of rivets corresponds to a small roughness density $F_r/F = 0.02$, for which, according to figure 18 of the Schlichting report, the drag coefficient for roughness elements similar to rivet heads is independent of the roughness density and is the same as for single rivets.

The measurements on a row of countersunk rivets arranged oblique to the stream direction show only a slight dependence of C_w on the stream direction for the pitches investigated.

Thus one may conclude from the preceding experimental results that countersunk rivets in any arbitrary arrangement at pitches common in practice barely influence one another and therefore the coefficient for the rivets measured singly may be taken as a basis for the calculations.

This rule cannot be applied directly to other rivet head types. In contrast to countersunk rivets, flat head rivets have a far reaching wake since this depends essentially on the parameter D/h for cylindrical roughness elements, so that for the common pitches a small drag decrease is to be expected. For consecutive rows of round head or brazier head rivets the statements made for the faired flat ridge are valid.

Figures 11 and 12: The drag of a hexagon nut depends only slightly on the stream direction and the distance from the leading edge. If one considers two nuts, one behind the other, in comparison with corresponding countersunk rivets, one finds that the geometric form has an effect upon the mutual influence of disturbance bodies.

Figure 13: It is clear that a lap joint parting against the stream produces a larger drag than the triangular profile. Rigorously one can compare directly only C_w values between $\alpha = 3^0$ and 4^0 since in this region the $Re(h)$ numbers (5×10^3) agree.

Figures 14 and 17: The few experimental points which, in reference 1, were obtained for circular and groove-shaped cavities do not show which quantities determine the resistance. Supplementary measurements made for other depth ratios and other positions relative to the front of the test plate showed a dependence of the drag coefficients on the two parameters $-h/D$ or $-h/t$ and D/δ or t/δ. In the case of circular cavities a periodic variation in drag coefficients with a pronounced maximum at $-\dfrac{h}{t} \approx 0.5$ was confirmed. On the other hand groove-shaped cavities showed only one maximum (but a very sharp one) at $-\dfrac{h}{t} \approx 0.1$.

The stream patterns published by Wieghardt illustrate the flow over two-dimensional rectangular cavities. In narrow grooves vortices lie one under the other. (See top sketch.)
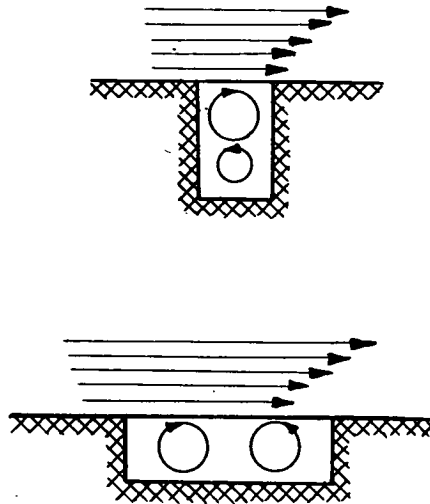
The fluid passing over them cannot disturb the stability of the system and it contributes to the support of the rotation the necessary energy which manifests itself as drag. On the other hand the vortices in wide grooves are side by side. The outer stream along the wall, determined essentially by the boundary layer thickness δ, effects the distruction of this formation. The results are vortex separation and therefore high Δc_w values.

Moreover the stream conditions at rectangular grooves seem to be rather independent of the length of the groove since the values for the full-span transverse slot fit quite well in the graph.

Figures 15 and 16: The drag coefficients of partly covered (in experiment, by 1 mm-thick, sharp-edge plate) cavities have been obtained based both on the plan area of the submerged cavity and on the area of the opening. Covered circular holes, in contrast to open ones, show less drag for the same opening d.

Figures 18 and 19: The partly covered and the open box-shaped cavities have about the same drag for the same surface opening.

Figures 20, 21, and 22: For bent cover plates the drag curves at both gap ratios are essentially alike. Since they show especially

sharp minima at $\alpha_V \approx 0°$, the position of the minima depending only slightly on the α_H values, small changes in the angle α_V have a large effect on the drag. If one bends the rear plate only about $5°$ inward (pattern B, fig. 22), one obtains a drag reduction of 20 percent to 25 percent, with only slight further reduction for the further improved design forms (C, D). The same result was found for beveled and rounded corners (F, G, and H).

Figures 23, 24, and 25: For comparison, the drag of box-shape grooves measured without covers, but with built-in lips (Δw without cover given in fig. 18), has been used. For evenly raised covers the drag of the suspension was estimated according to reference 1. The pressures, which were measured at the four measuring places in the bottom of the box-shaped groove, barely differ from one another. The mean value, referred to the dynamic pressure of the undisturbed stream, is given in figure 24. In order to gain an insight into the flow between the box and the uniformly raised cover the velocity profiles over the rear edge at $z = 0$ and 125 millimeters were measured. The smaller the height of the cover the more the fluid streaming through is retarded. From the good agreement of the related profiles one can conclude that the stream passing through is essentially two dimensional except in the immediate neighborhood of the lateral edges.

Figure 26: The dimples were tested for three different stream directions, in order to get a clear understanding as to how one best forms cavities of least drag. In accord with the above-mentioned facts the values are strongly dependent on the ratio t/δ.

5. EXAMPLE OF APPLICATION

In an example the use of the experimental results on an actual situation will be illustrated. The nomograms plotted in reference 1 will be used for the determination of δ, $\bar{q}$, and $\log Re(h)$.

Example: 2 weld seams, one behind the other.

U = 700 kilometers per hour

X = 1.6 meters

$\dfrac{UX}{\nu} = 2.2 \times 10^7$
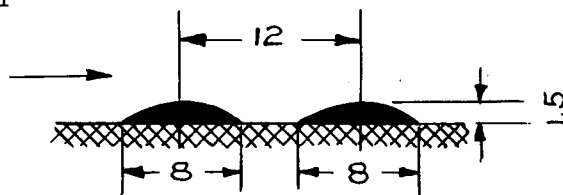
From the nomogram: $\delta \approx 20$ millimeters

   Weld seam (faired flat ridge):

   h = 1.5 millimeters $\frac{h}{t} = 0.19$ $\frac{h}{\delta} \approx 0.075$

   t = 8 millimeters

From the nomogram: $\overline{q} \approx 880$ kilograms per millimeter^2, log Re(h) ≈ 4.1.

At such large Re(h)-numbers the drag of the ridges could, for practical reasons, no longer be measured. One can estimate the value, however, by extrapolating on figure 8a

$$C_w(B/t \rightarrow \infty) \approx 0.1$$

Separation of the weld seams:

$$B/t = 1.5$$

According to figure 8:

$$\frac{C_w}{C_w(B/t \rightarrow \infty)} - 1 \approx 0.7$$

$$C_w \approx 0.17$$

   Therewith the additional drag of the two weld seams, one behind the other, amounts to

$$\Delta w \approx 0.17 \times 880 \times 1.5 \times 10^{-3} \text{ kilogram per meter} \approx 0.22 \text{ kilogram per meter}$$

6. SUMMARY

   The increase of the turbulent friction drag of a flat plate due to various surface disturbances, which were investigated to complete earlier measurements by K. Wieghardt, is reported. The additional drags may be resolved into the pressure drag of the disturbance and the change in the surface friction drag of the plate. If the first part is independent of the Reynolds number and the second is relatively small compared to the first, it is hypothesized that the generalized drag coefficient C_w, which has been obtained in the boundary layer, has the same value as in the free stream. Study of the application of this idea to rectangular plates indicates satisfactory agreement.

The measurements on continuously rounded elements, faired flat ridges, and hoods confirmed again the presence of critical drag decreases in the turbulent boundary layer. The drag coefficients show, therefore, a strong dependence on the $Re(h)$-number and on the surface curvature of the single roughness element.

Surface disturbances arranged one behind the other have, in general, a drag that decreases as the separation distance decreases. An exception, however, exists for rounded protuberances for flow slightly above the critical $Re(h)$-number; here there is a certain distance of separation at which the second protuberance is at a sub-critical $Re(h)$-number in the wake of the first protuberance and therefore shows a greater drag than the first. This result was found for two faired flat ridges, one behind the other, and may probably be applied generally to single roughness elements not having sharp edges producing separation. At $Re(h)$ greatly exceeding $Re_{critical}$ this special behavior is not to be expected. As was shown in a practical example, at the high velocities of flight, even on protuberances of small height, the above-critical flow condition occurs and by proper arrangement of the surface disturbances one can considerably reduce the detrimental drag increases.

Rows of countersunk rivets, investigated in several arrangements, barely influenced each other since the wakes dissipated within the pitch distances commonly used in practice.

As the experimental results on circular and rectangular cavities showed, the drag of cavities is determined by the two parameters $-h/t$ and t/δ. The drag curves show, at a certain depth ratio $-h/t$ which depends on the geometric form of the cavity, a pronounced maximum, the value of which increases with t/δ. An attempt was made to decrease the drag by special modifications of the edges of the cavity (for example, projecting plates, beveled or rounded corners, etc.). A dimple was tested for different flow directions in order to obtain a clear basis for the construction of cavities having the least drag.
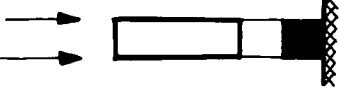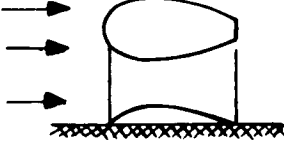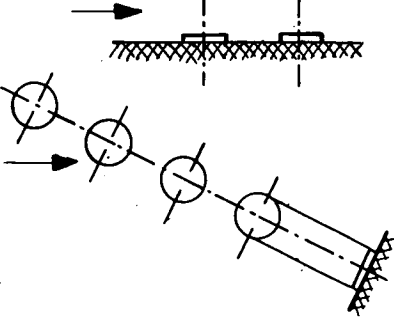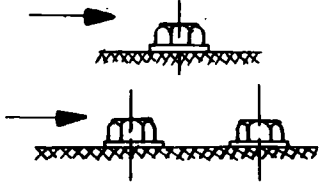
Furthermore some drag measurements are presented for special disturbances, parted lap joints, and cavities with covers.

Translated by Hugh C. Du Bose
National Advisory Committee
for Aeronautics
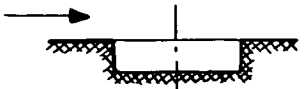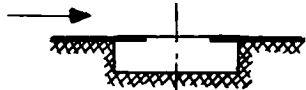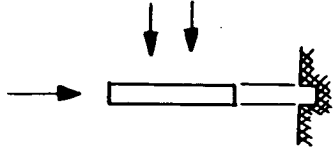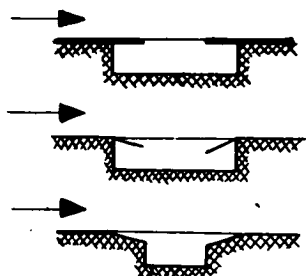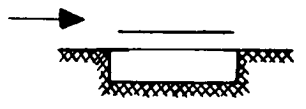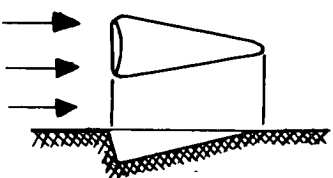
7. REFERENCES

1. Wieghardt, K.: Erhöhung des turbulenten Reibungswiderstandes durch
   Oberflächenstörungen. ZWB Forschungsbericht 1563, March 19, 1942.
   (Also Jahrb. d. Deutsch. Luftfahrtforsch. 1943.)

2. Flachsbart, O.: Messungen an ebenen und gewölbten Platten. AVA-
   Ergebn. IV. Lief., 1932, p. 96.

3. Engelhardt, H.: Zusatzwiderstände durch Ansetzen von Halbdrehkörpern
   an eine ebene Wand. Bericht 5/43 des Aerodynamischen Laboratoriums
   der T. H. München.

4. Schlichting, H.: Experimentelle Untersuchungen zum Rauhigkeits-
   problem. Ing.-Arch. Bd. VII, No. 1, 1936, p. 1. (Available
   as NACA TM 823.)

Designation of the Irregularities Investigated

	Square plates normal to flow	Figures 1,2
	Square bars of varying length in flow direction	Figure 3
	Drag coefficients of similar roughness elements	Figure 4
	Hoods Lengths varied Profile varied Width of afterbody varied	 Figure 5 Figure 6 Figure 7
	Two faired flat ridges one behind the other	Figure 8
	Single faired flat ridge	Figure 8a
	Two rows of countersunk rivets one behind the other Row of countersunk rivets oblique to direction of flow	Figure 9 Figure 10
	Hexagonal nut with washer Two hexagonal nuts one behind the other	Figure 11 Figure 12
	Parting lap joint	Figure 13

Designation of the Irregularities Investigated (Continued)

	Circular cavity	Figure 14
	Partly-covered circular cavity	Figures 15, 16
	Slot-shaped cavity	Figure 17
	Box-shaped cavity, partly covered	Figures 18, 19
	Different edge shapes	Figures 20, 21, 22
	Box-shaped cavity with various cover plates	Figures 23, 24, 25
	Dimple	Figure 26
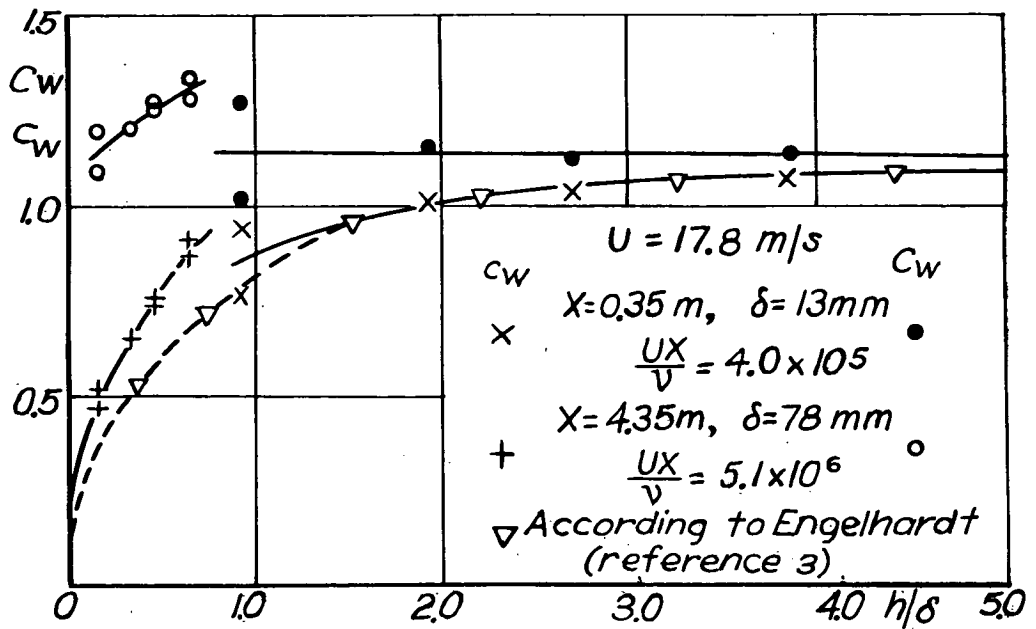
Figure 1.- Square plates normal to flow direction; c_w and C_w as functions of h/δ.
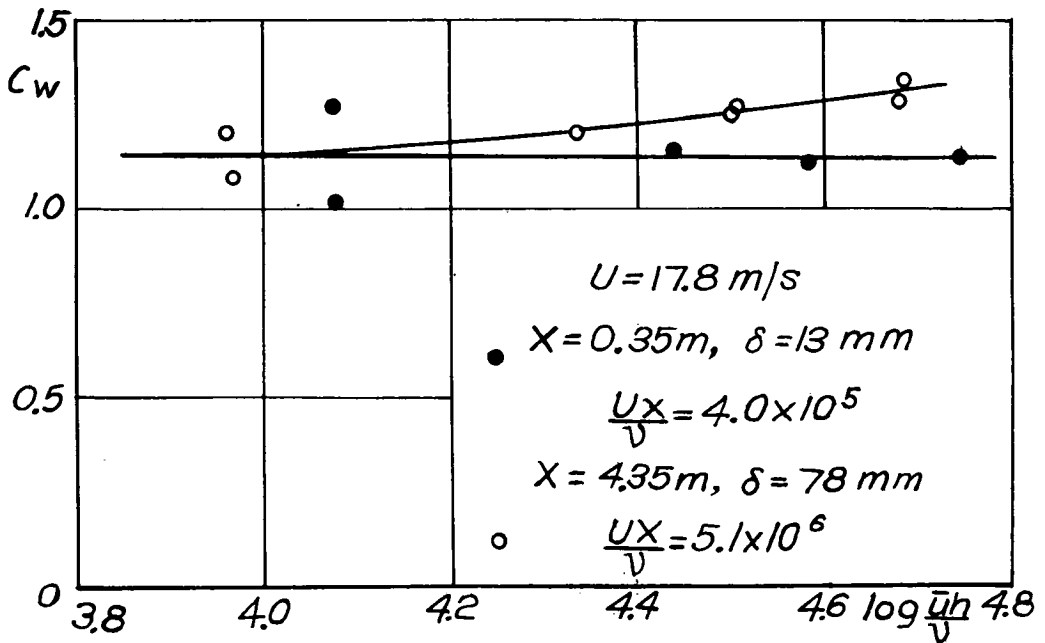
Figure 2.- Square plates normal to flow direction; C_w as function of $\log Re\,(h)$.
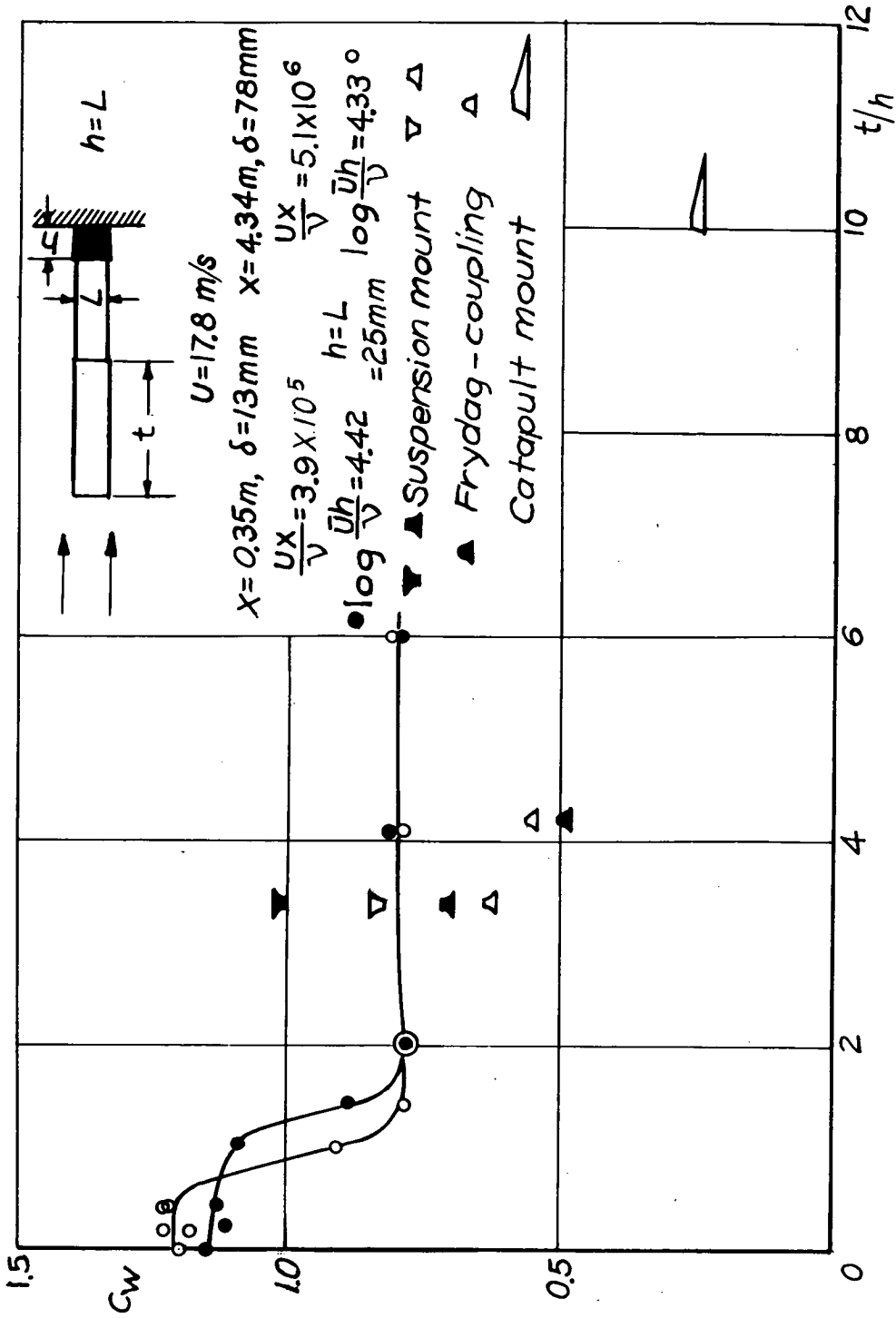
Figure 3.- Square bars of various lengths in the flow direction; comparison with similar roughness elements.

$U = 17.8\,m/s$

	$X = 0.35\,m$	$X = 4.35\,m$
	$\delta = 13\,mm$	$\delta = 78\,mm$
	$\dfrac{UX}{v} = 4.0 \times 10^5$	$\dfrac{UX}{v} = 5.1 \times 10^6$

M 1:2

$f = 500\,mm^2$

	$X = 0.35\,m$	$X = 4.35\,m$
c_w	0.91	0.46
$C_{w\,\bar{u}h}$	1.03	0.85
$\log \dfrac{\bar{u}h}{v}$	4.44	4.34

Suspension mount

$f = 486\,mm^2$

c_w	0.63	0.34
C_w	0.72	0.64
$\log \dfrac{\bar{u}h}{v}$	4.44	4.34

Only for theoretical comparison

M 1:2

$f = 611\,mm^2$

c_w	0.44	0.30
C_w	0.50	0.56
$\log \dfrac{\bar{u}h}{v}$	4.44	4.37

Frydag - coupling

M 1:2.5

$f = 1200\,mm^2$

c_w	0.16
C_w	0.26
$\log \dfrac{\bar{u}h}{v}$	4.51
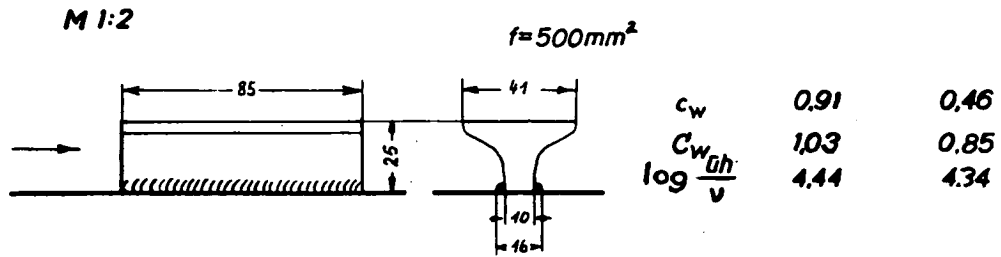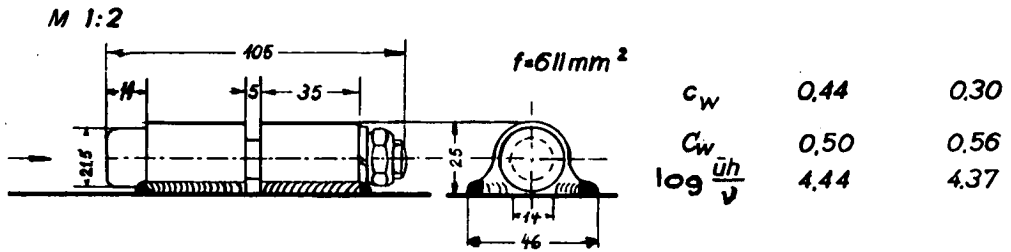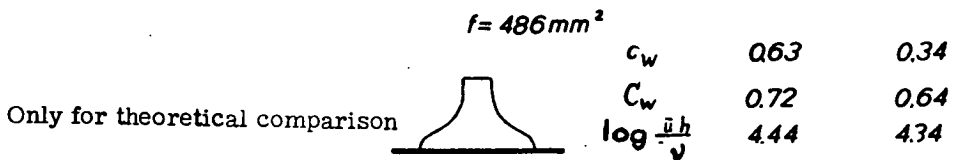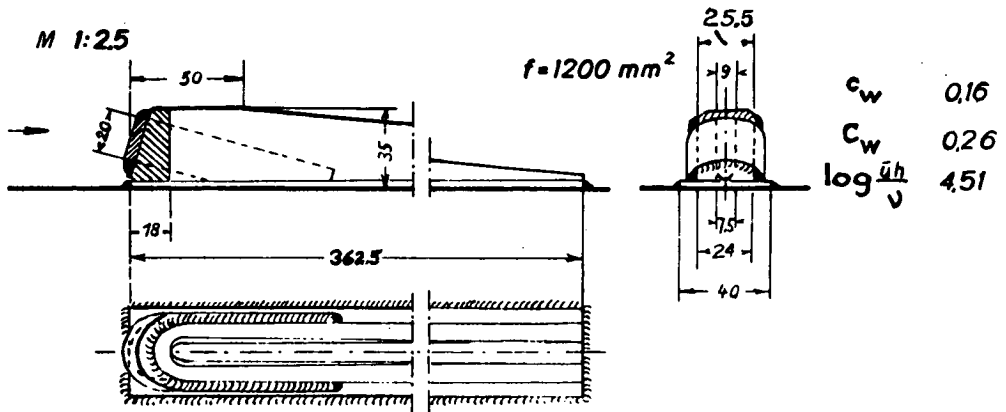
Catapult mount

Figure 4.-   Drag coefficients of various special roughness elements.
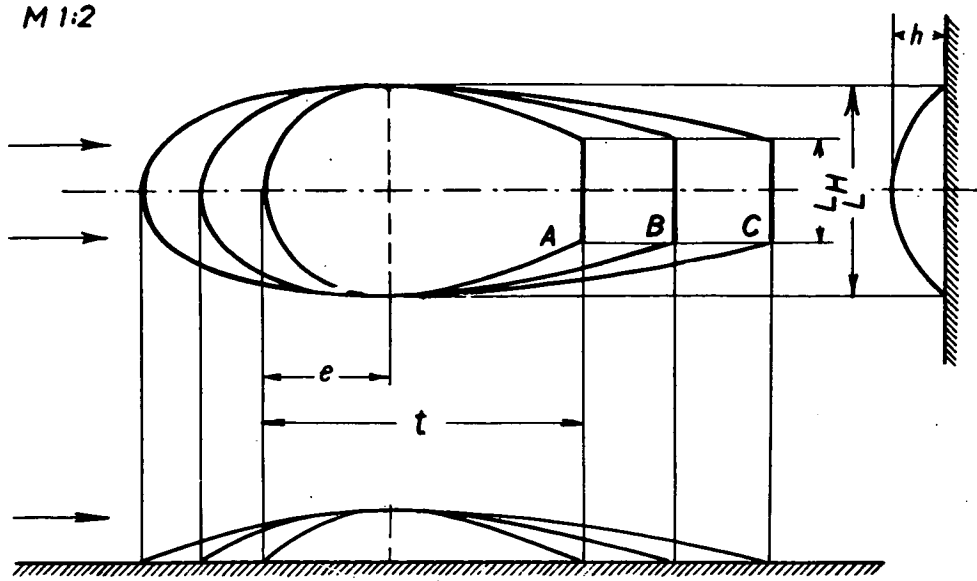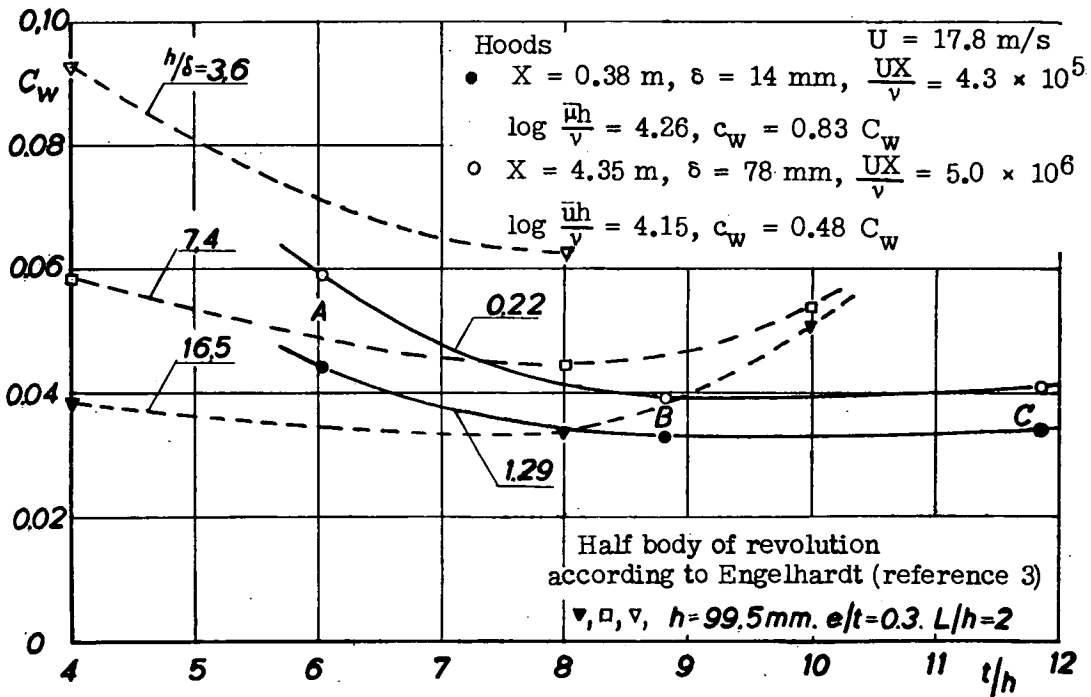
Figure 5.- Hoods of various lengths, e/t = const.
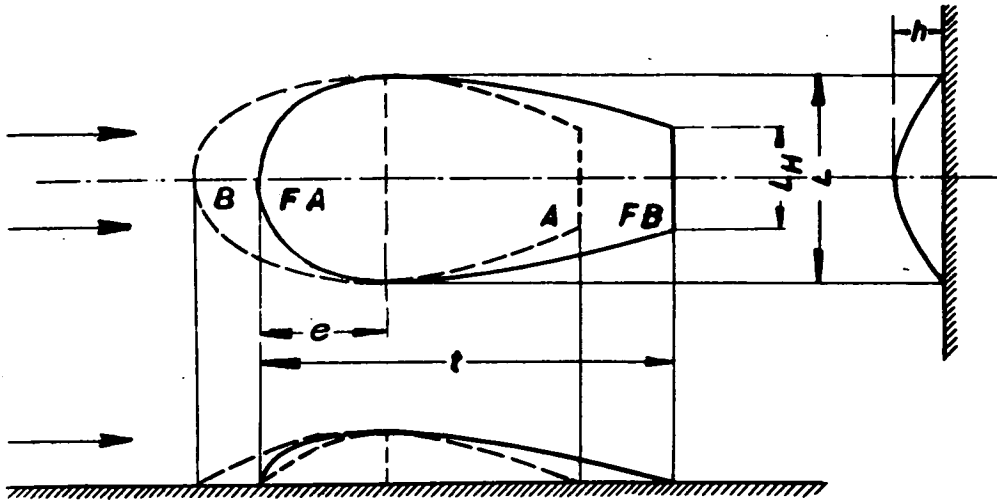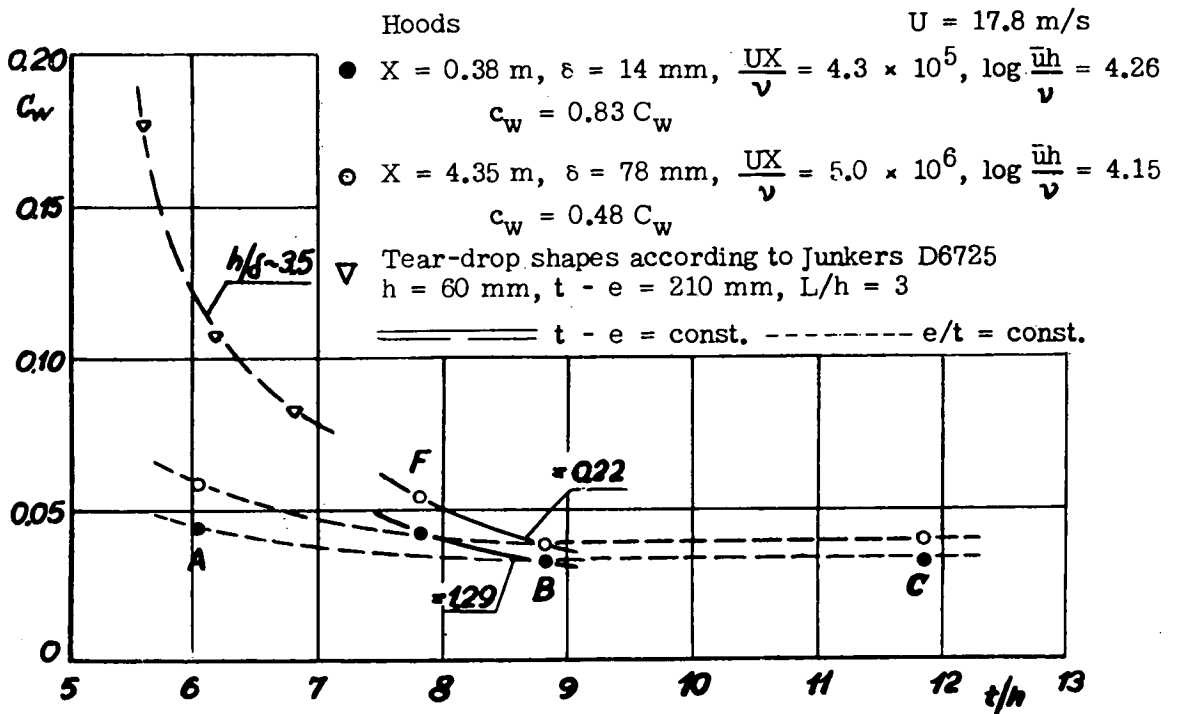
Figure 6.- Hoods of various profiles.

M 1:2
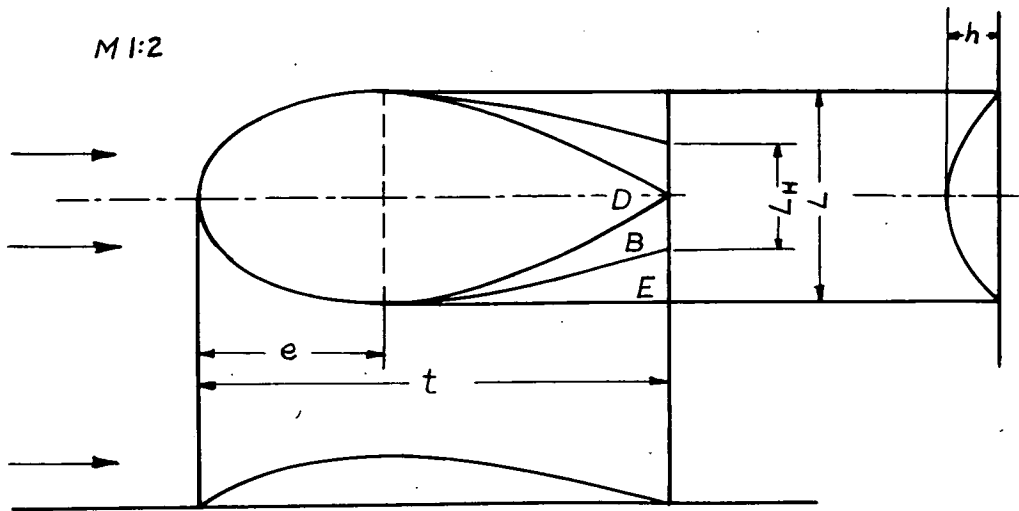
$e/t = 0.4$ $t/h \approx 9$ $L_H|L = 0; 0.5; 1$ $h = 17mm$

$L/h = 4$ $f = 800mm^2$

Hoods $U = 17.8\ m\ s$
$X = 0.38\ m,\quad \delta = 14\ mm,$
$\dfrac{Ux}{v} = 4.3 \times 10^5,\ log\ \dfrac{\bar{U}h}{v} = 4.26,$
$c_w = 0.83\ C_w,$

$X = 4.35\ m,\ \delta = 78\ mm,$
$\dfrac{Ux}{v} = 5.0 \times 10^6,\ log\ \dfrac{\bar{U}h}{v} = 4.15$
$c_w = 0.48\ C_w,$

Half-body of revolution
according to Engelhart
(reference 3)
$h = 99.5\ mm$
$e/t = 0.3\quad t/h = 4$
$L/h = 2$
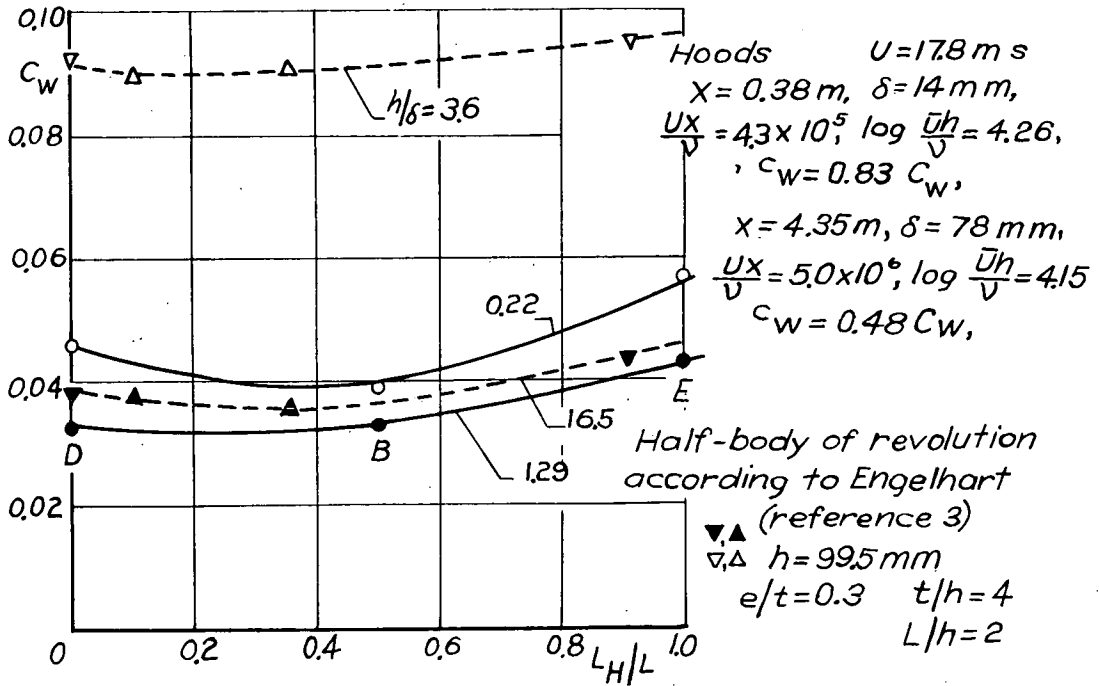
Figure 7.- Hoods of various afterbody widths.
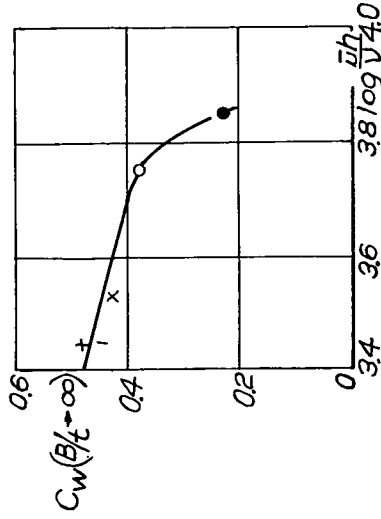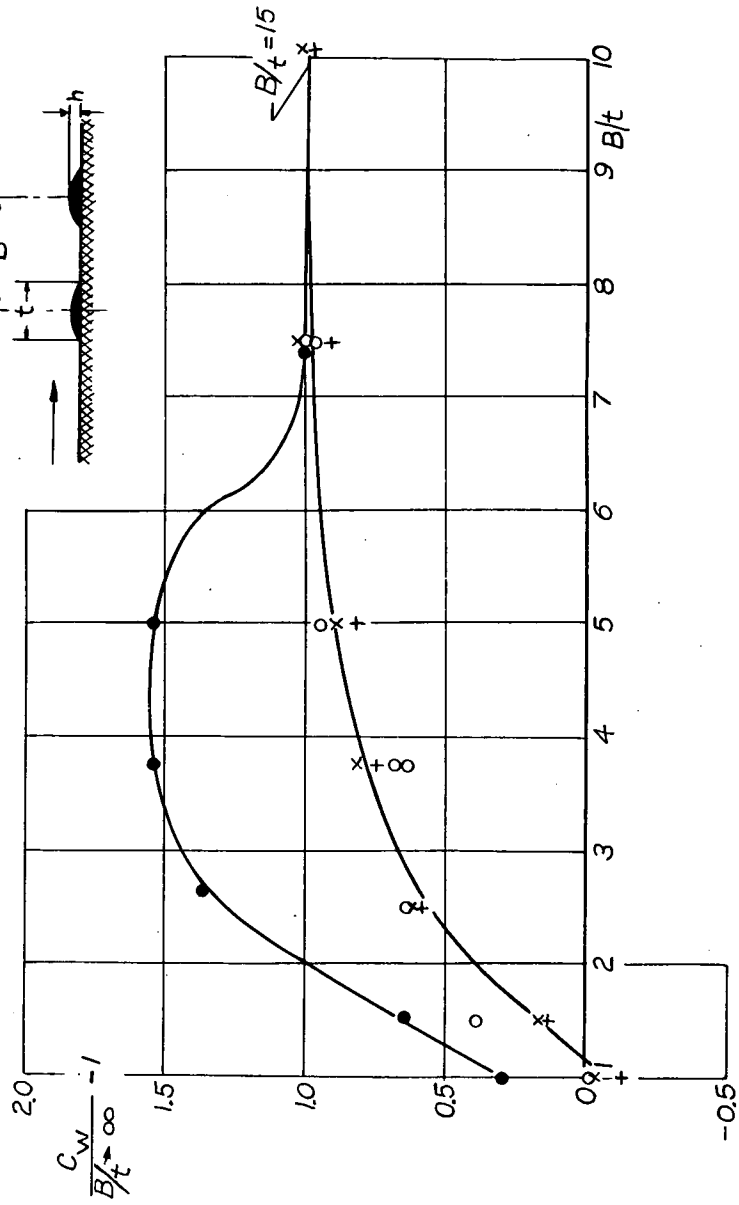
Figure 8a.- Single faired flat ridges.

Figure 8.- Two faired flat ridges lying one behind the other.
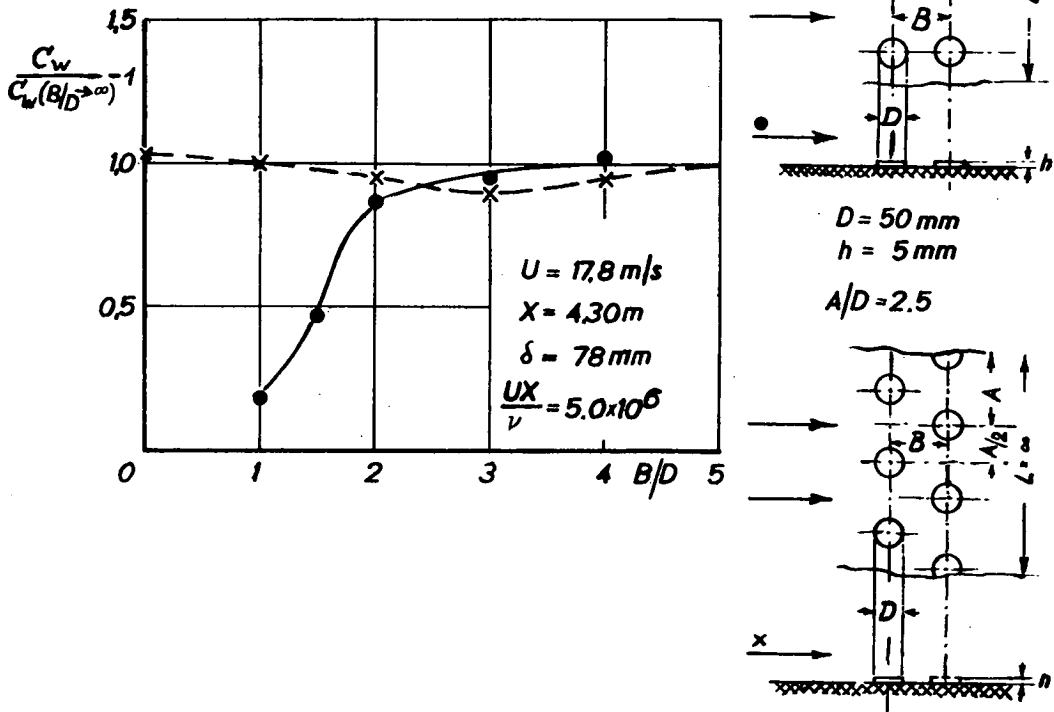
Figure 9.- Two rows of countersunk rivets one behind the other.
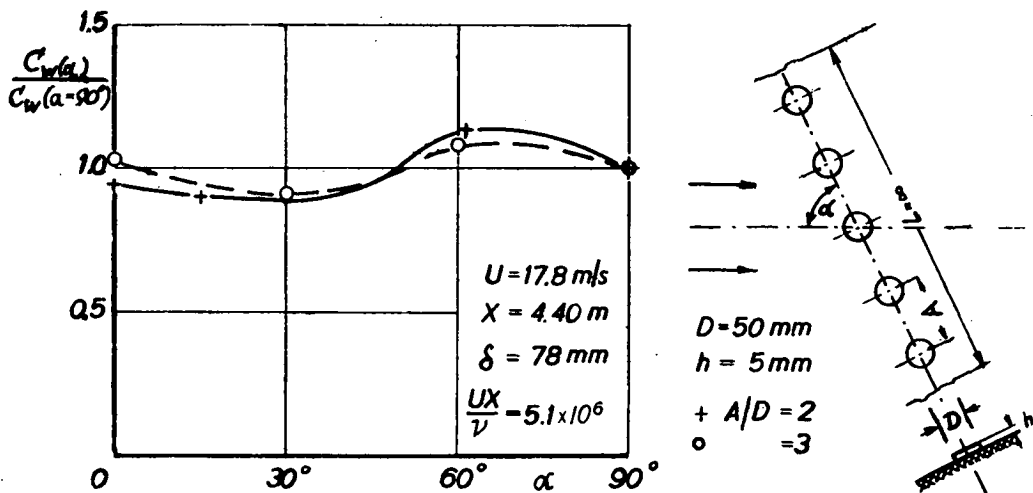
Figure 10.- Row of countersunk rivets oblique to flow direction.
Single countersunk rivet: $C_w = 0.49$

$\left(U = 17.8 \text{ m/s}, \quad X = 4.35 \text{ m}, \quad \delta = 78 \text{ mm}, \quad \frac{UX}{\nu} = 5.0 \times 10^6, \log\frac{\bar{u}h}{\nu} = 4.33\right)$

$U = 17.8 \ m/s$

$X = 0.35 \ m; \quad \delta = 13mm \qquad X = 4.35 \ m; \quad \delta = 78mm$

$\dfrac{UX}{\nu} = 4.0 \times 10^5; \ \log \dfrac{\bar{u}h}{\nu} = 4.32 \qquad \dfrac{UX}{\nu} = 5.1 \times 10^6; \ \log \dfrac{\bar{u}h}{\nu} = 4.22$

$c_w = 0.85 \ C_w \qquad\qquad c_w = 0.50 \ C_w$
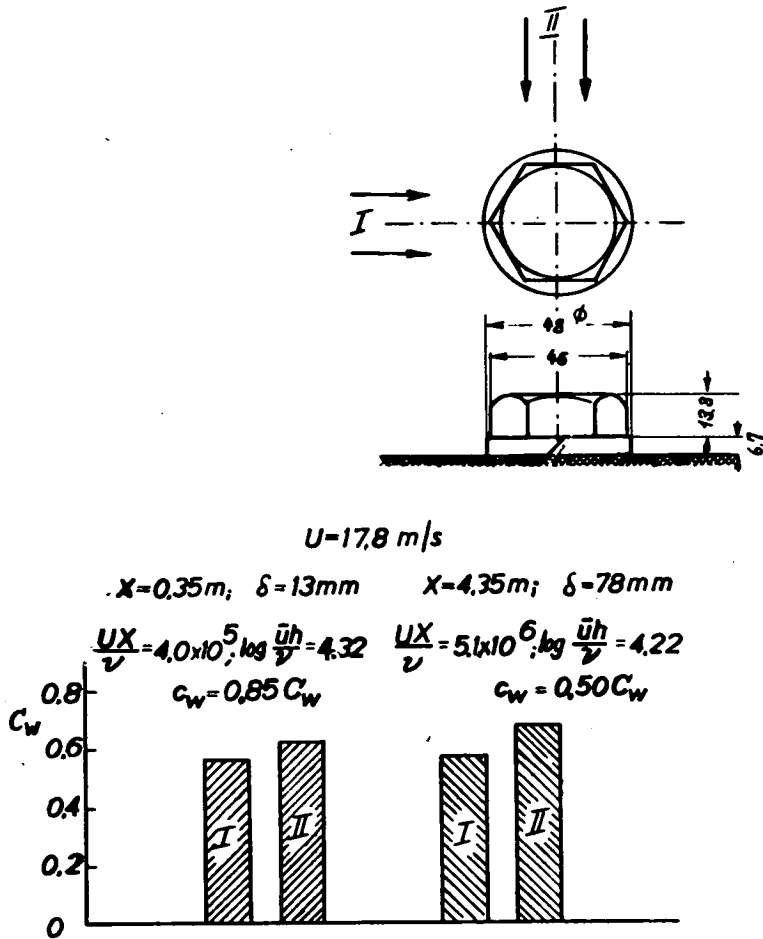
Figure 11.- Hexagonal nut with lock washer.

$U = 17.9 \ m/s$

$X = 4.32 m$

$\delta = 78mm$

$\dfrac{UX}{\nu} = 5.0 \times 10^6$

$h = 20mm$

$D/h = 2.4$
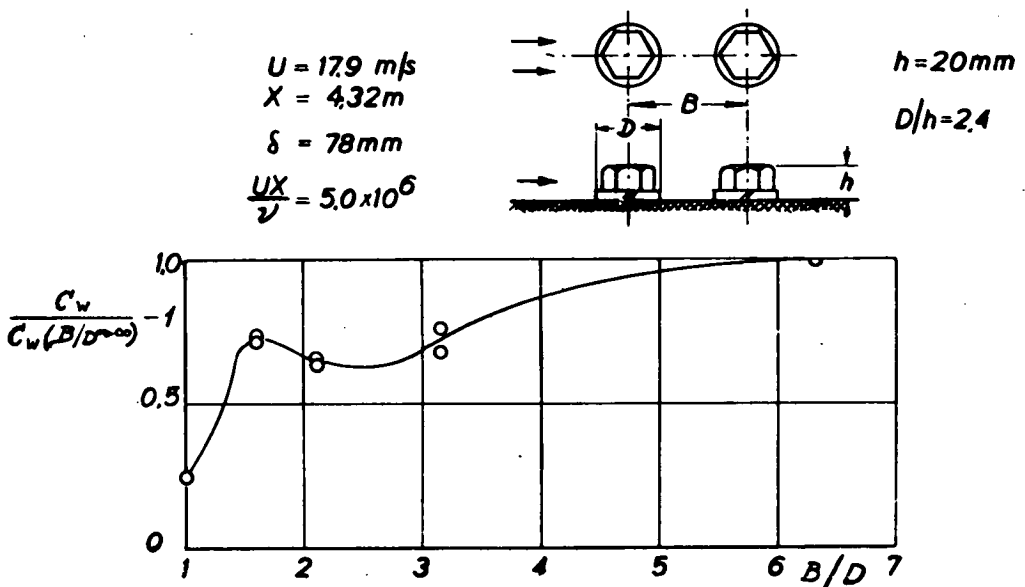
Figure 12.- Two hexagonal nuts one behind the other.
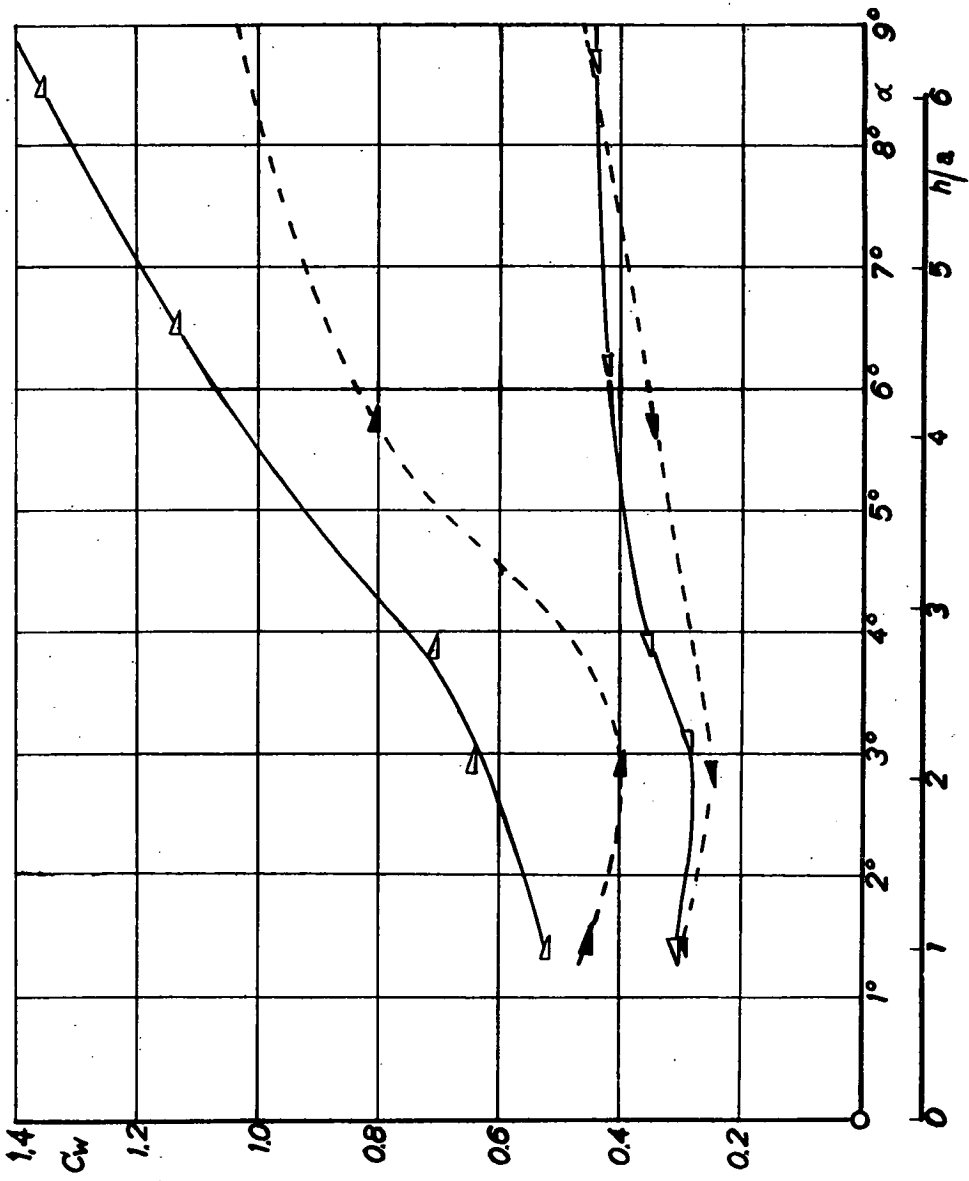
Figure 13.- Parting lap joint, comparison with triangular profile of Wieghardt
(reference 1).
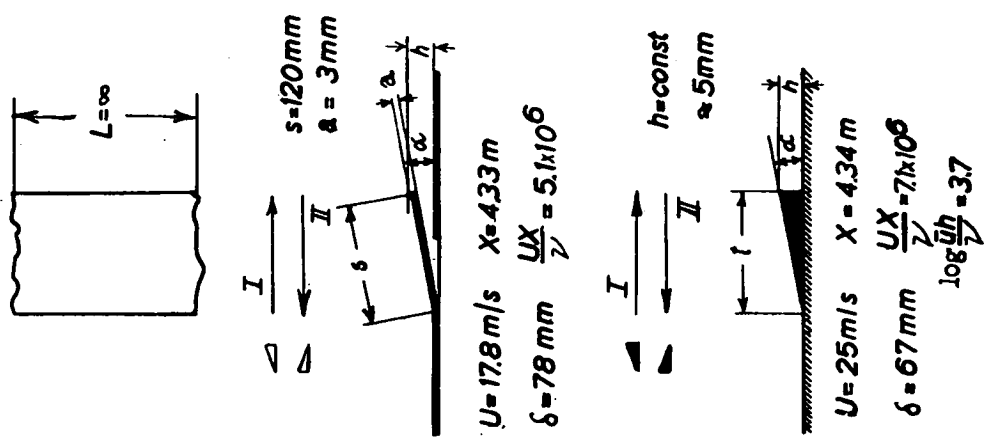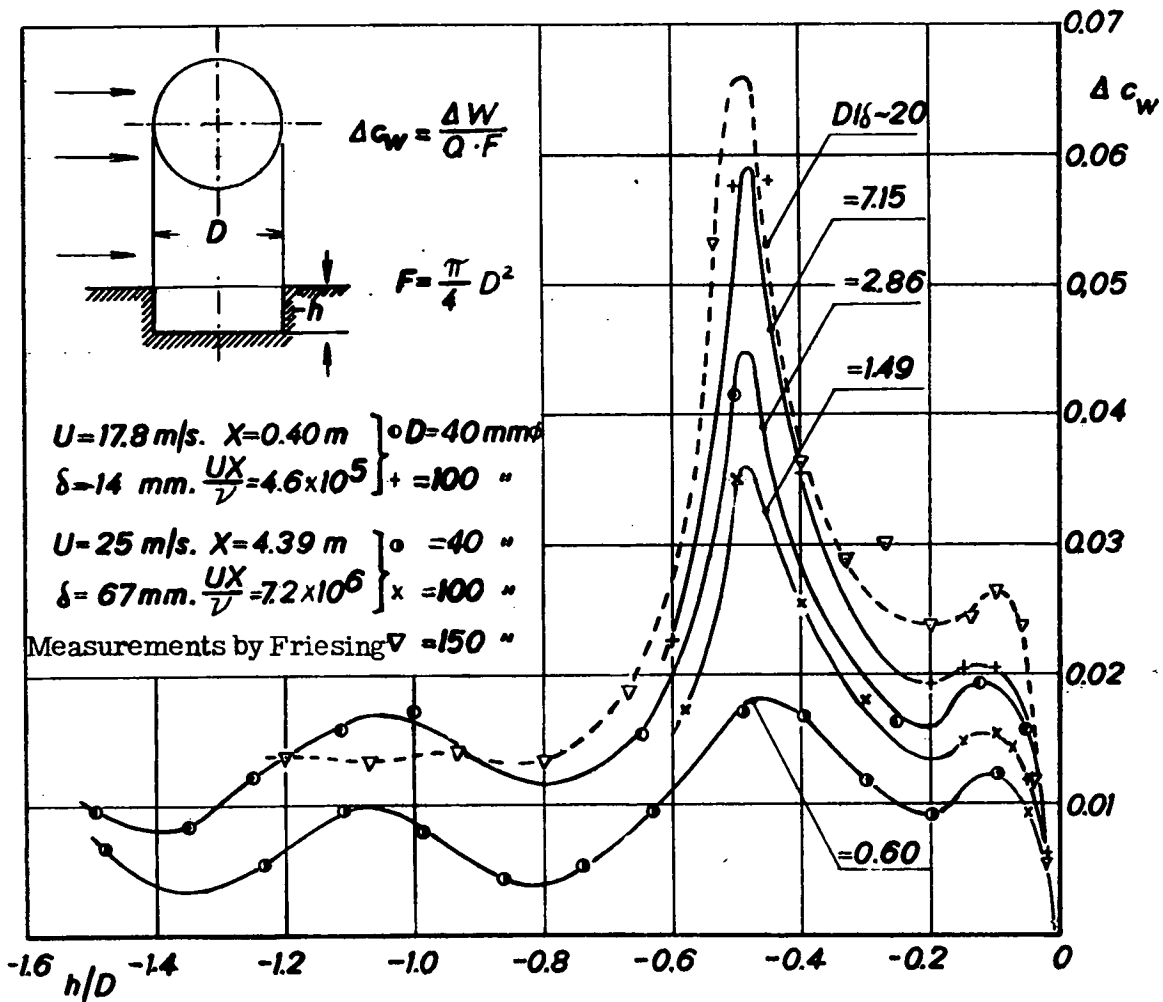
Figure 14.- Circular cavities.
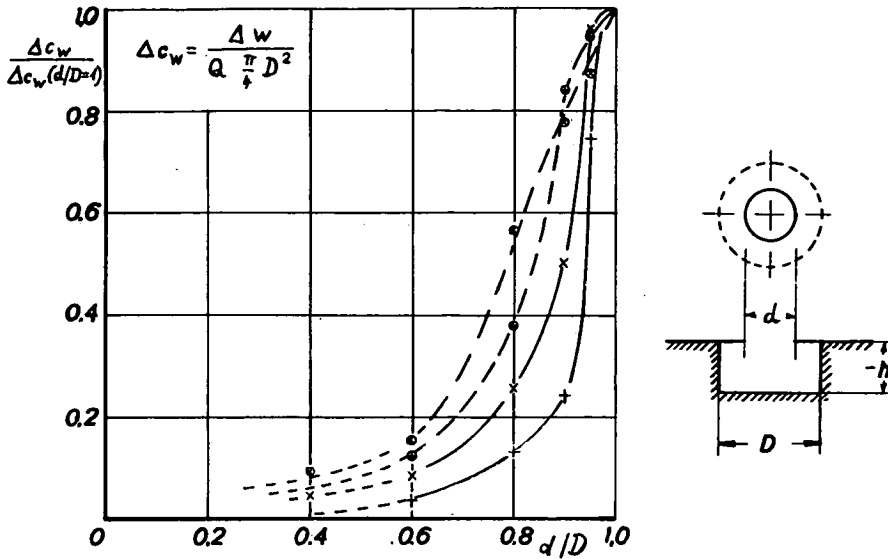
Figure 15.- Circular covered cavities of varying opening ratio.
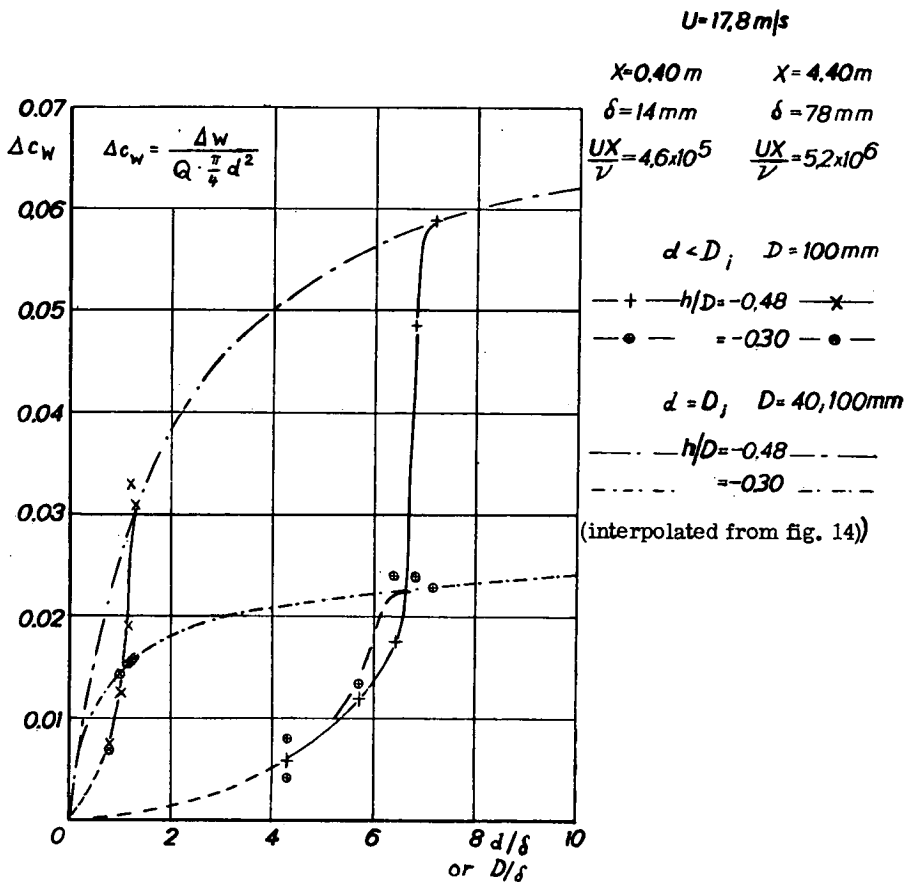
Figure 16.- Comparison of open and partly covered circular cavities.
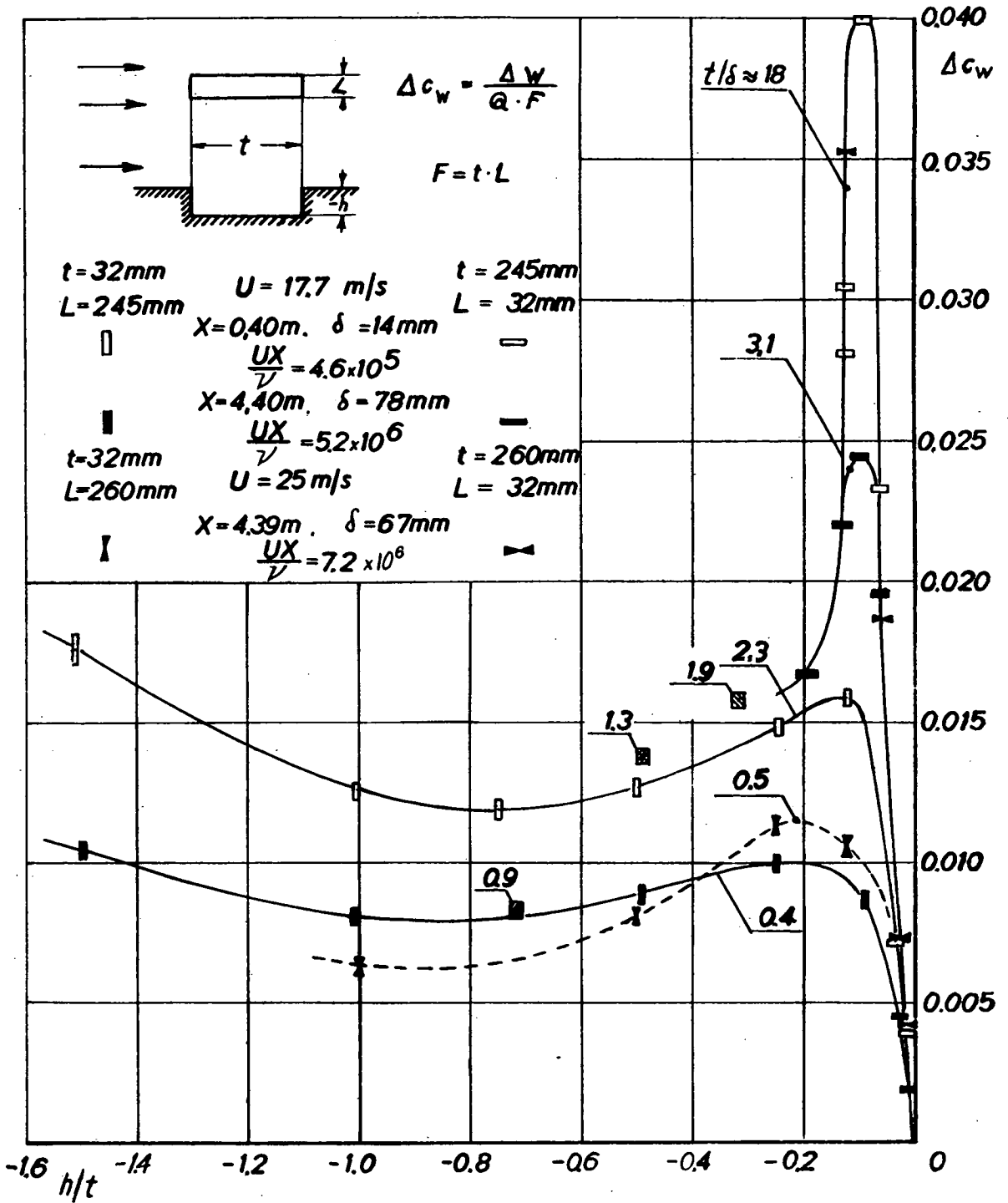
Figure 17.-   Slot-shaped cavities. (Box-shaped cavities   L = 300 mm,
t = 150 mm,   t = 100 mm,   t = 70 mm).
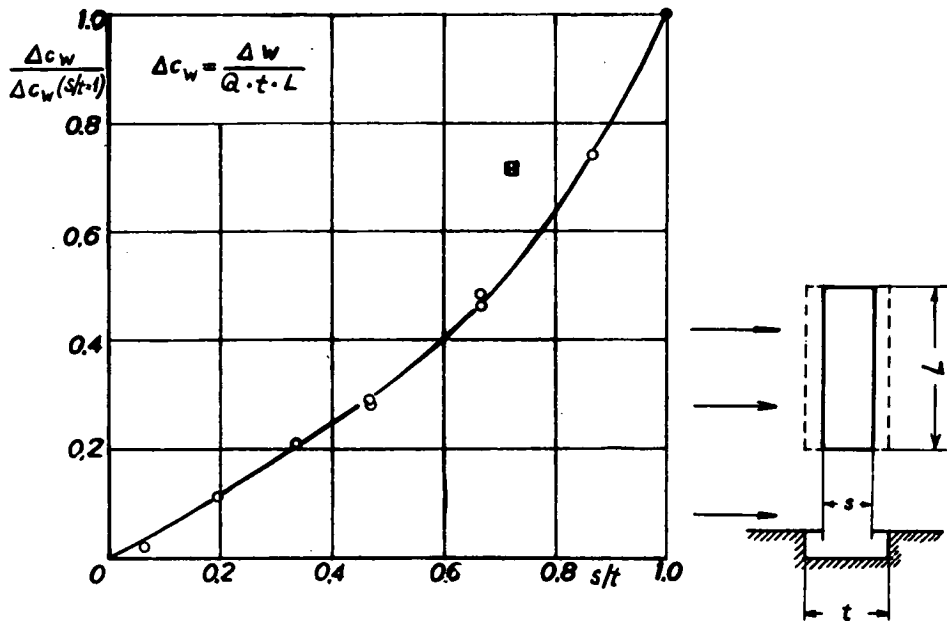
Figure 18.- Box-shaped cavities (t = 150 mm), with various opening ratios.
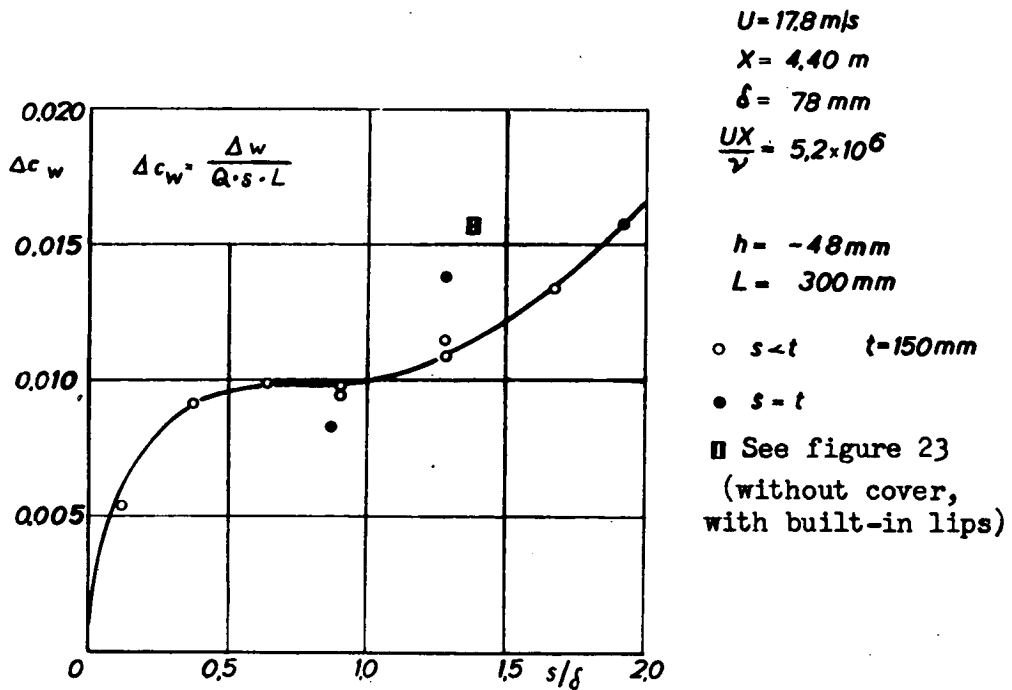
Figure 19.- Comparison of open and partly closed box-shaped cavities.
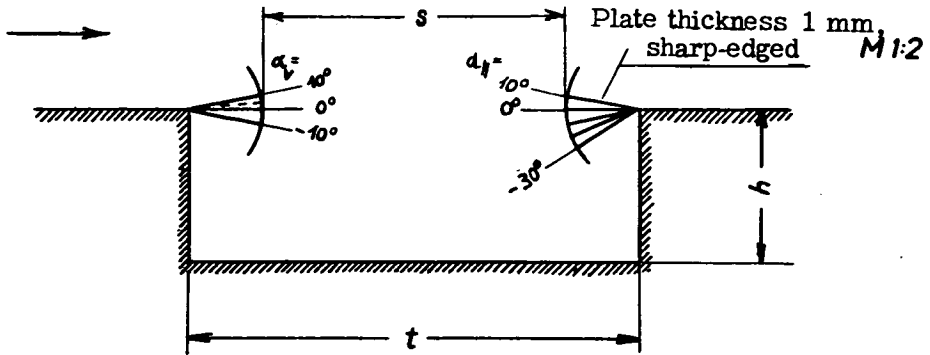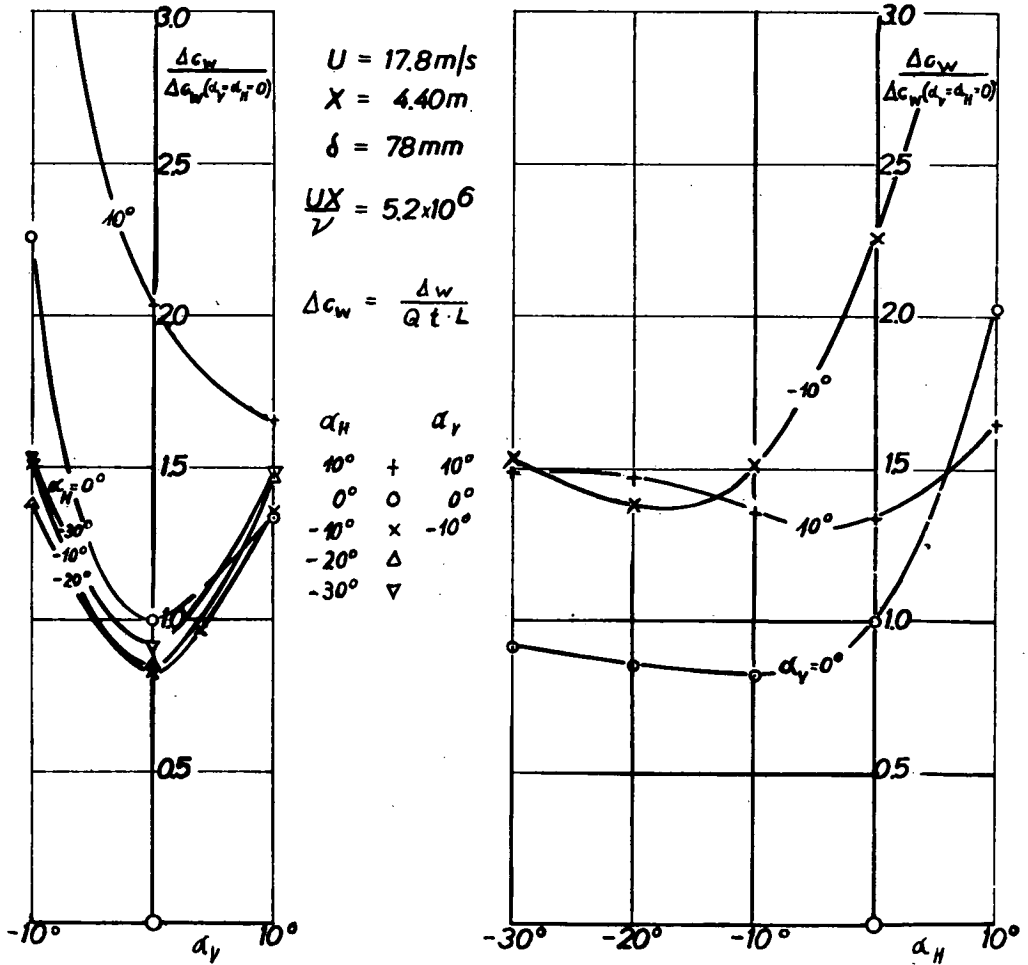
Figure 20.-   Box-shaped cavities with edge plates at various angles (s/t ≈ 0.7).
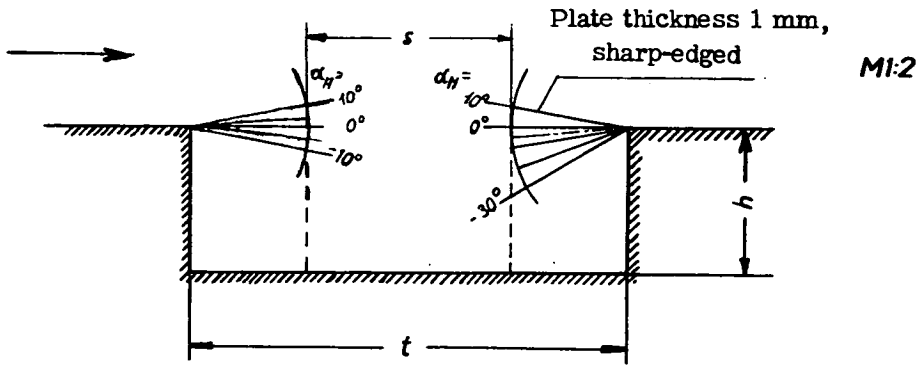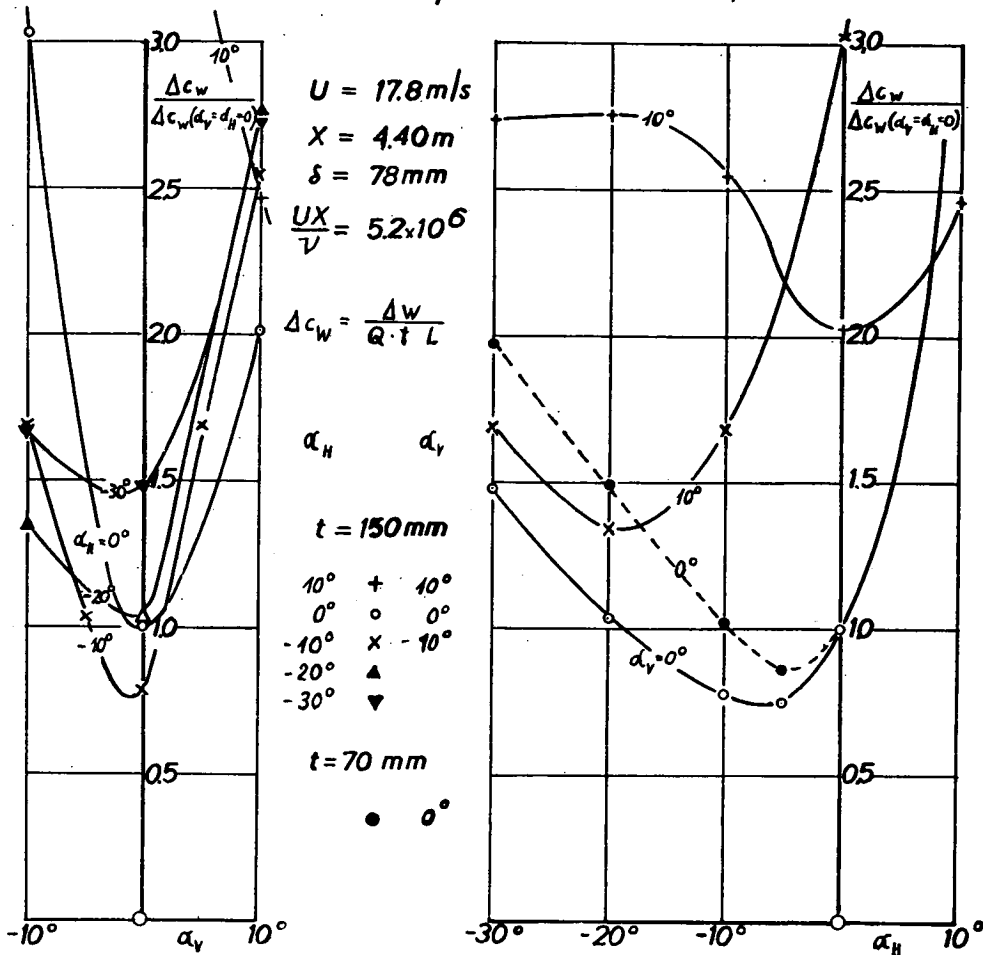
Figure 21.-   Box-shaped cavities with edge plates at various angles (s/t ≈ 0.5);
Comparison with beveled edges.
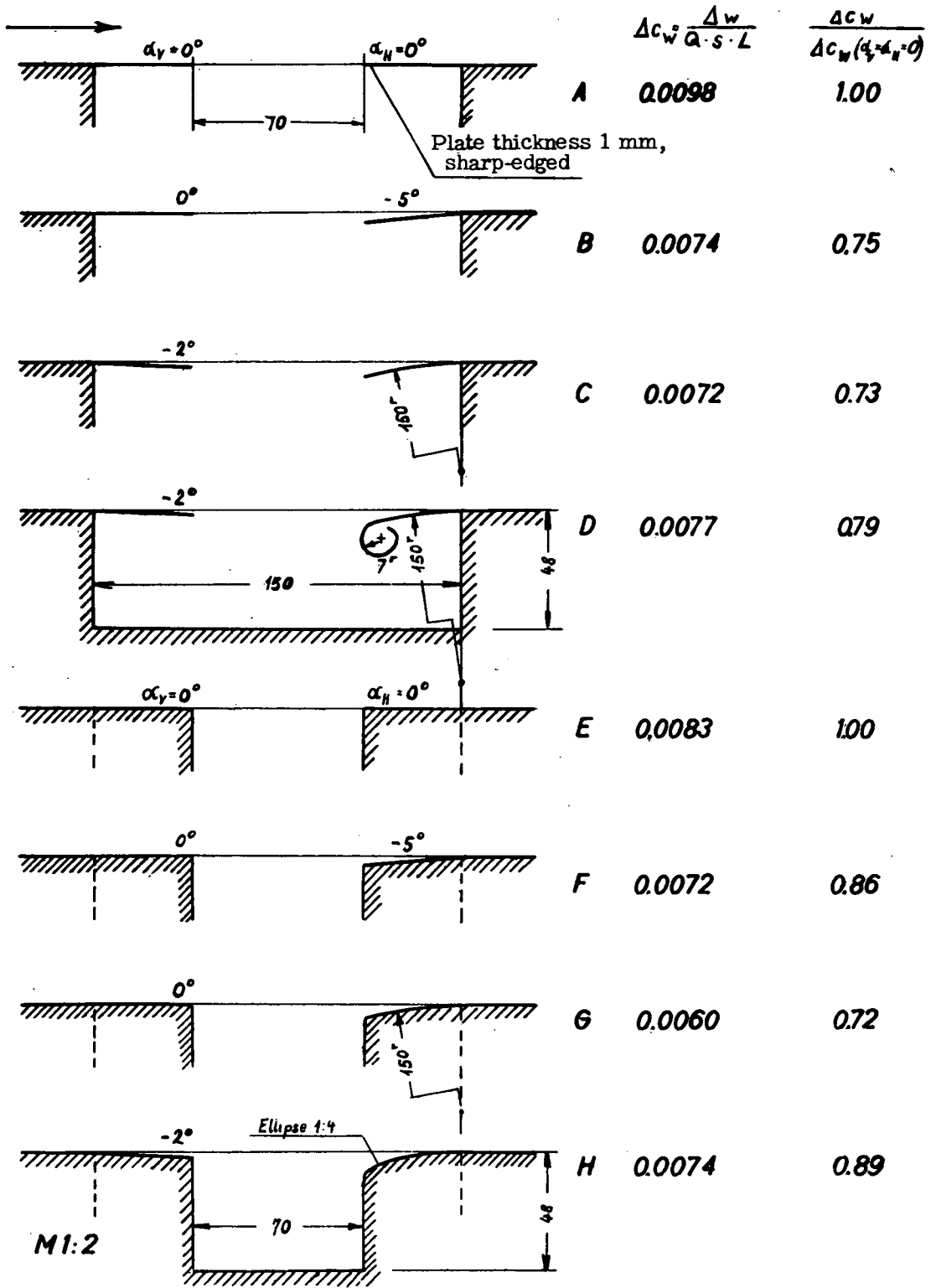
Figure 22.-   Drag coefficients of box-shaped cavities with several selected
edge shapes.

M 1:2
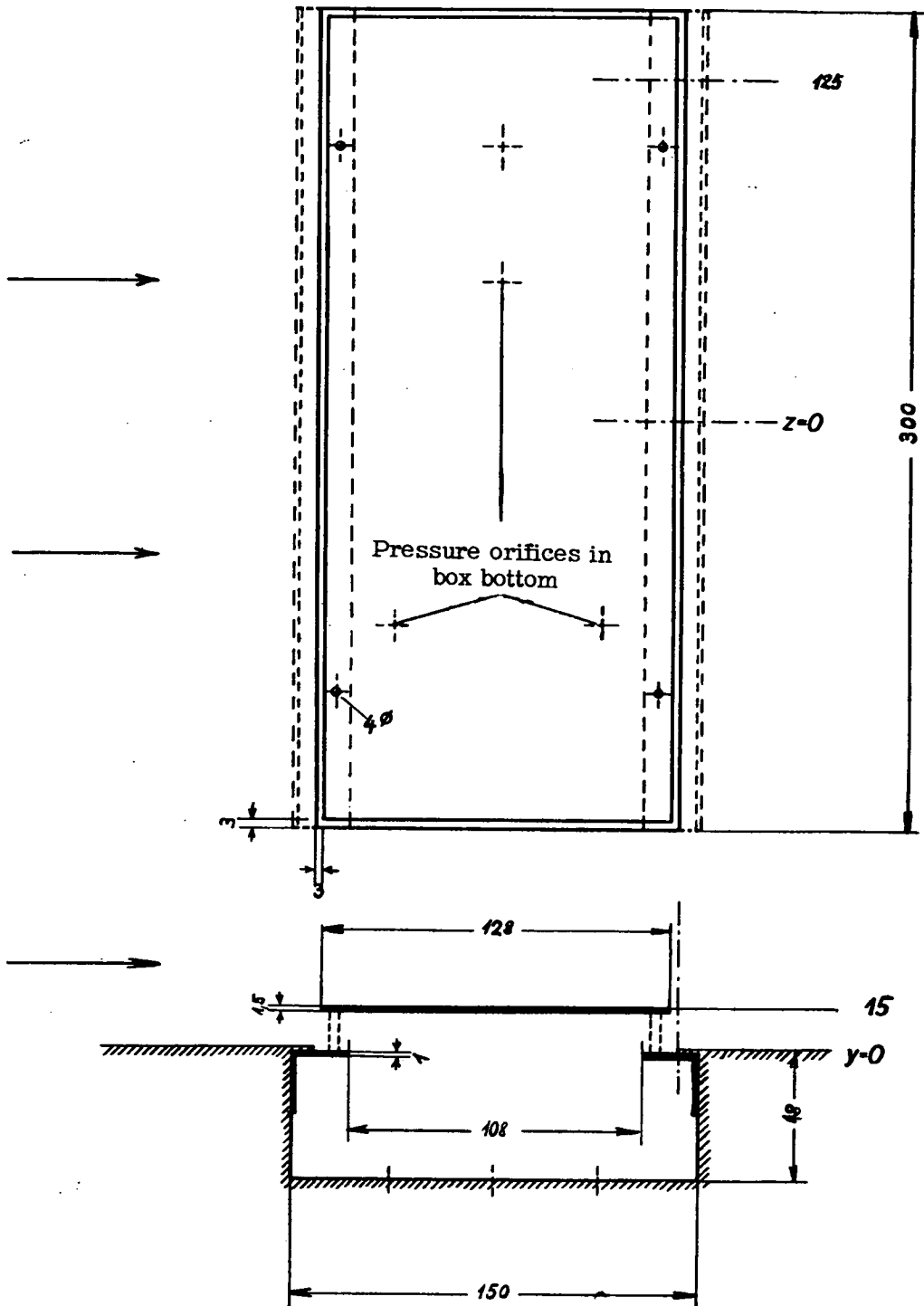
Figure 23.- Dimensions of box-shaped cavity with cover (e.g. cover evenly
raised).
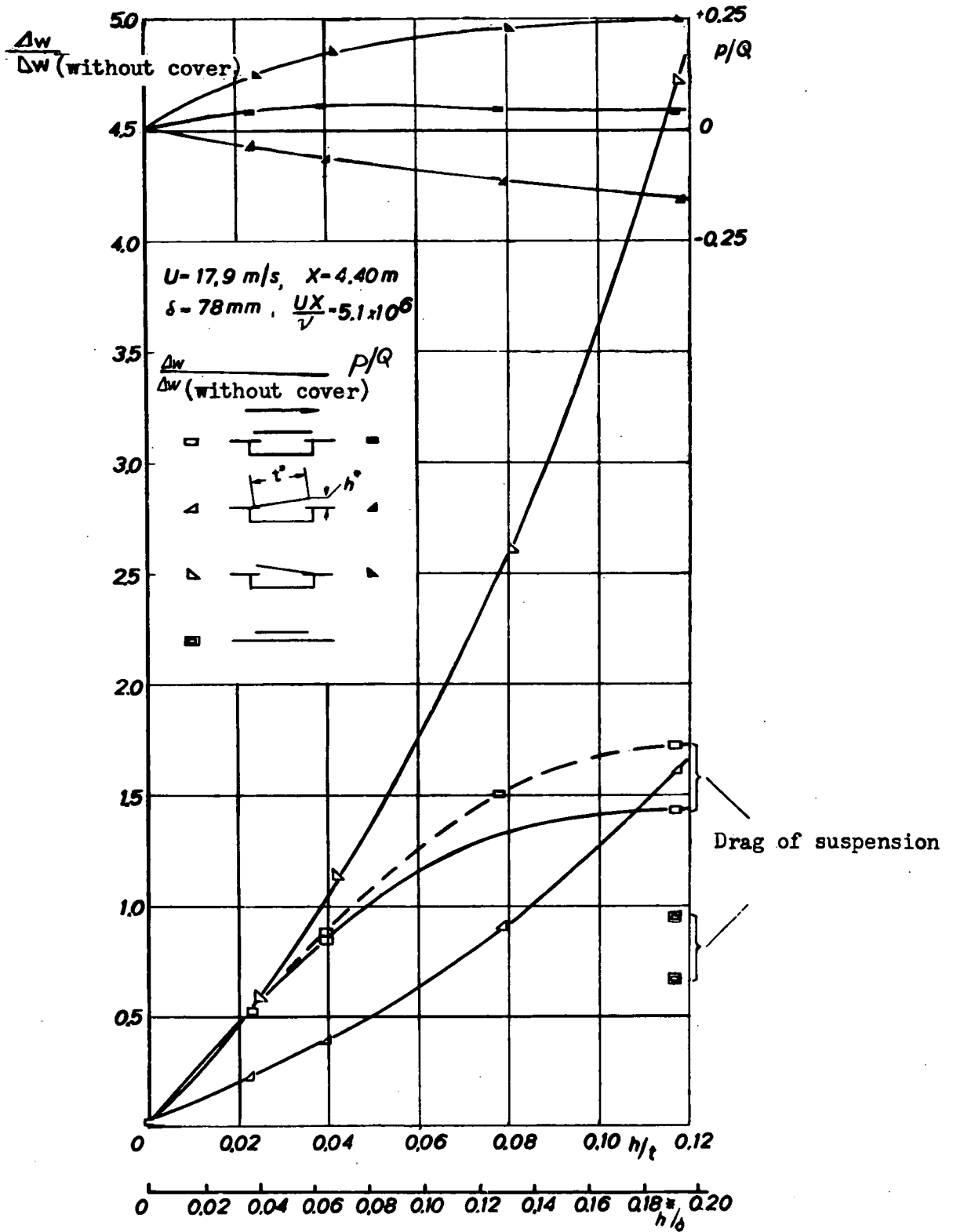
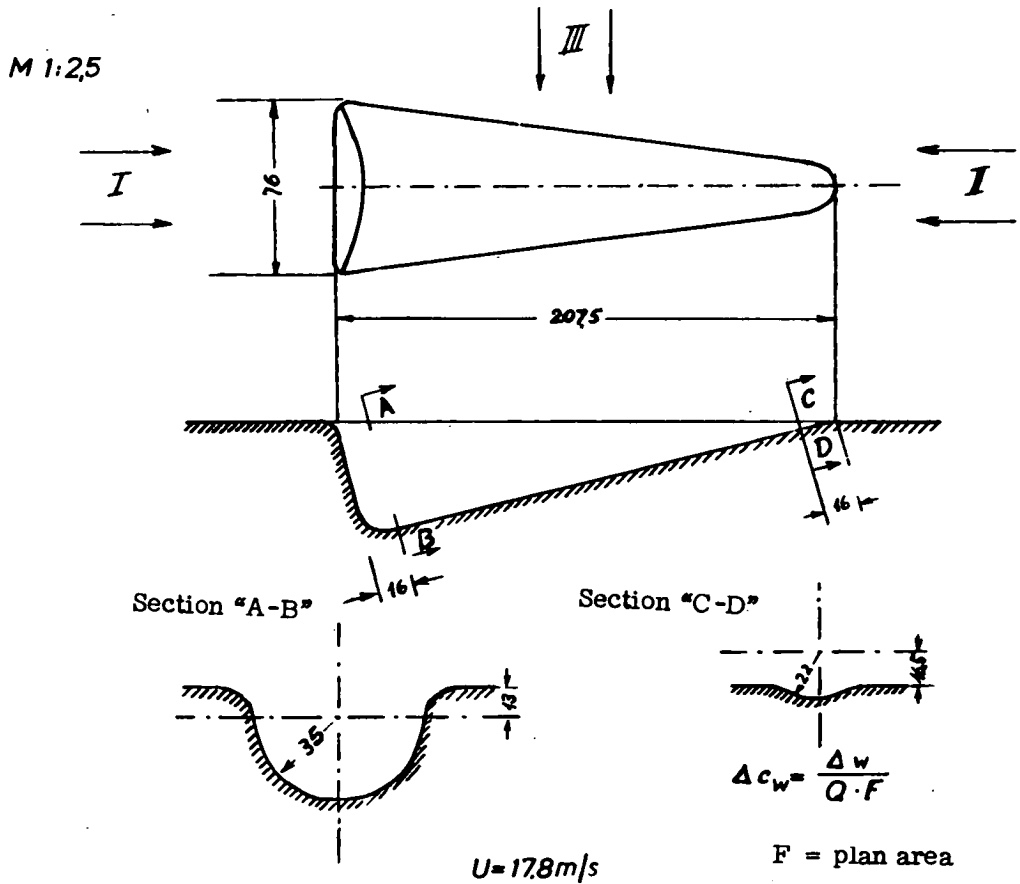Figure 24.- Box-shaped cavity with various cover arrangements.
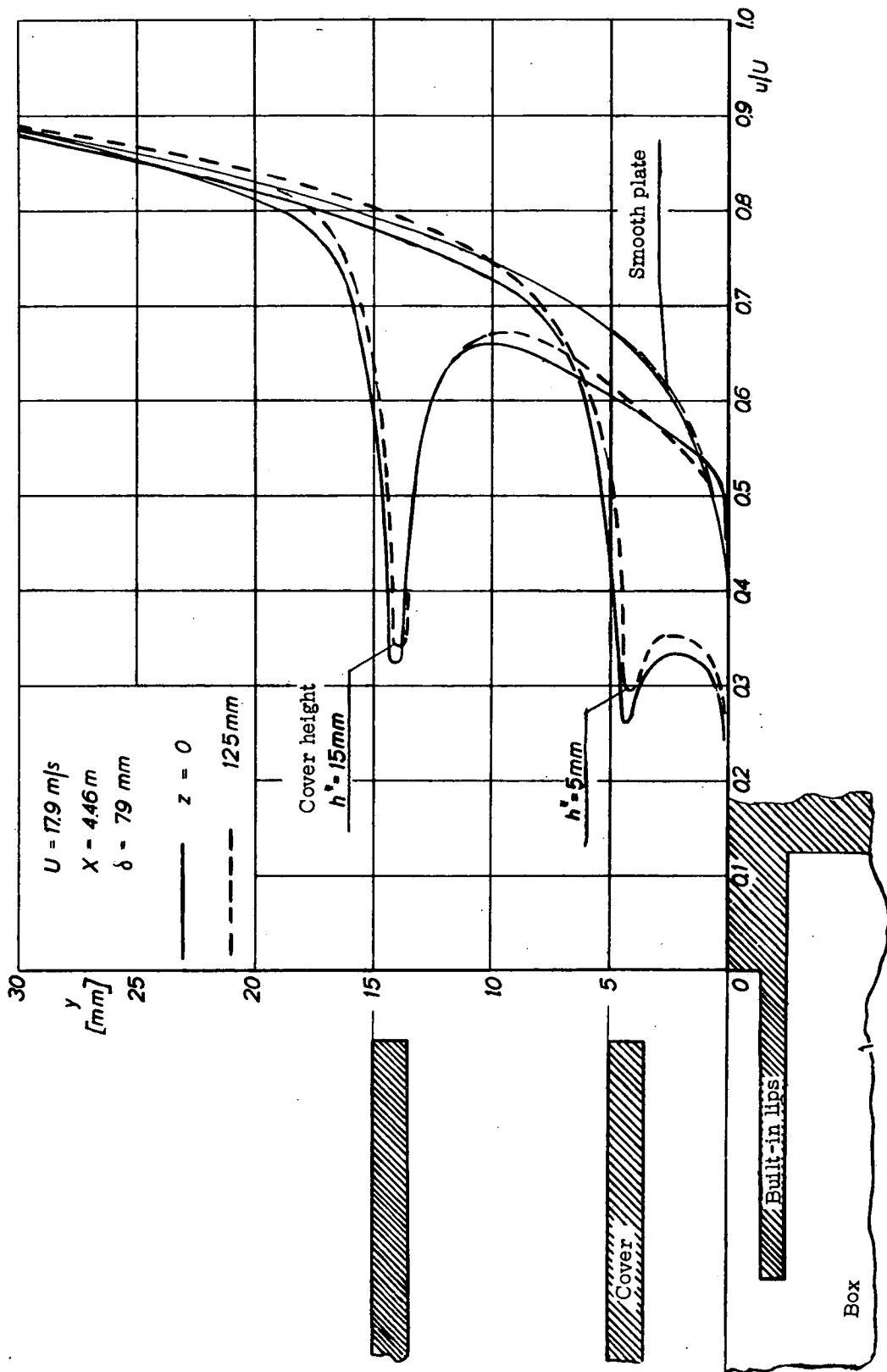
Figure 25.- Velocity profile behind box-shaped cavity with evenly raised cover.
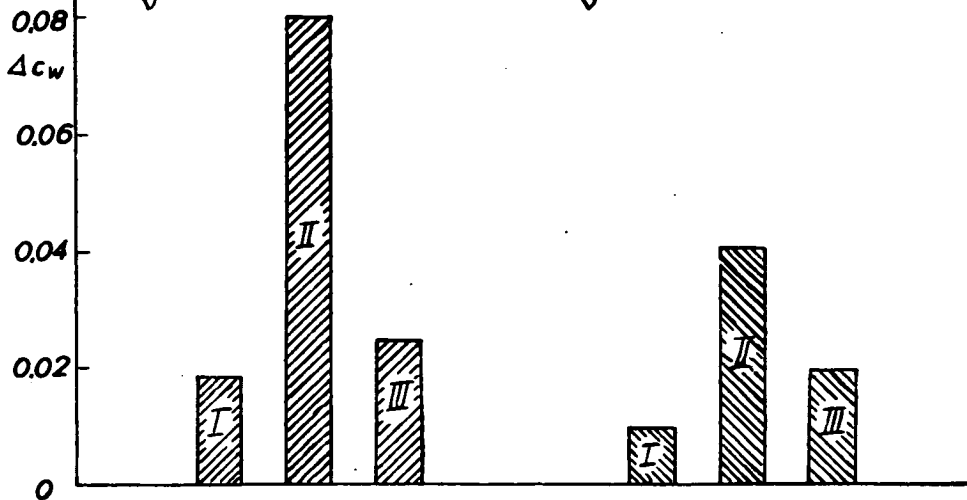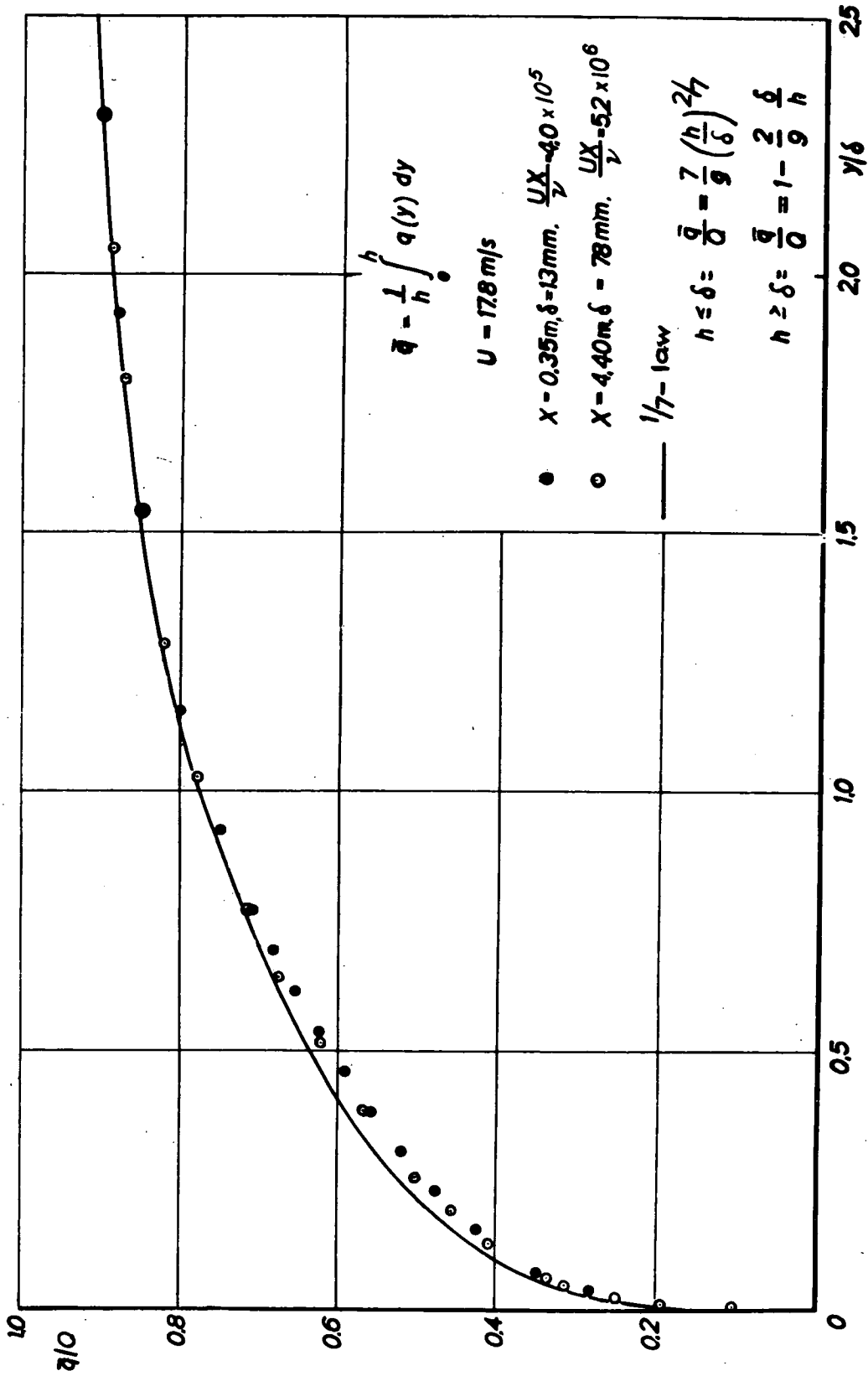
Figure 26.- Dimples.

Figure 27.- Mean dynamic pressure in the boundary layer.